We are IntechOpen, the world's leading publisher of Open Access books Built by scientists, for scientists

5,600
Open access books available

137,000
International authors and editors

170M
Downloads

Our authors are among the

154
Countries delivered to

TOP 1%
most cited scientists

12.2%
Contributors from top 500 universities

WEB OF SCIENCE™

Selection of our books indexed in the Book Citation Index in Web of Science™ Core Collection (BKCI)

Interested in publishing with us?
Contact book.department@intechopen.com

Numbers displayed above are based on latest data collected.
For more information visit www.intechopen.com

Chapter

Lidar Observations in South America. Part II - Troposphere

Eduardo Landulfo, Alexandre Cacheffo, Alexandre Calzavara Yoshida, Antonio Arleques Gomes, Fábio Juliano da Silva Lopes, Gregori de Arruda Moreira, Jonatan João da Silva, Vania Andrioli, Alexandre Pimenta, Chi Wang, Jiyao Xu, Maria Paulete Pereira Martins, Paulo Batista, Henrique de Melo Jorge Barbosa, Diego Alves Gouveia, Boris Barja González, Felix Zamorano, Eduardo Quel, Clodomyra Pereira, Elian Wolfram, Facundo Ismael Casasola, Facundo Orte, Jacobo Omar Salvador, Juan Vicente Pallotta, Lidia Ana Otero, Maria Prieto, Pablo Roberto Ristori, Silvina Brusca, John Henry Reina Estupiñan, Estiven Sanchez Barrera, Juan Carlos Antuña-Marrero, Ricardo Forno, Marcos Andrade, Judith Johanna Hoelzemann, Anderson Guimarães Guedes, Cristina Tobler Sousa, Daniel Camilo Fortunato dos Santos Oliveira, Ediclê de Souza Fernandes Duarte, Marcos Paulo Araújo da Silva and Renata Sammara da Silva Santos

Abstract

In Part II of this chapter, we intend to show the significant advances and results concerning aerosols' tropospheric monitoring in South America. The tropospheric lidar monitoring is also supported by the Latin American Lidar Network (LALINET). It is concerned about aerosols originating from urban pollution, biomass burning, desert dust, sea spray, and other primary sources. Cloud studies and their impact on radiative transfer using tropospheric lidar measurements are also presented.

Keywords: lidar, LALINET, aerosols, atmospheric sciences, remote sensing, air quality, environment

1. Introduction

In Brazil, there are four lidar systems dedicated to the study of aerosols in the troposphere. Installed at Embrapa in Manaus (Western Amazon), there is a lidar system coordinated by the Atmospheric Physics Laboratory (LFA) of the Institute of Physics at the University of São Paulo [1]. In São Paulo, there are two other systems, the SPU Lidar Station, installed at the Institute of Energy and Nuclear Research (IPEN/CNEN) and coordinated by the Laboratory of Environmental Applications of Lasers (LEAL) hosted in the Center for Lasers and Applications (CELAP) of the referred institute, and the scanning lidar system located at CEPEMA (Centre for Training and Research in Environment) in Cubatão (State of São Paulo) [2–5]. **Figure 1** shows an example of the aerosol profile retrieved at SPU Station.

The DUSTER Lidar system, situated at the Department of Atmospheric and Climate Sciences (DCAC) at the Federal University of Rio Grande do Norte (UFRN), can measure marine aerosols' physical and optical properties. It can also measure aerosols (mineral dust) that cross the Atlantic Ocean and come from the desert Sahara, and aerosols originated from fires in the African continent [6, 7]. The lidar system's design and installation in Natal result from a technical and scientific collaboration among UFRN and IPEN. The DUSTER Lidar system is a biaxial monostatic lidar with a typical spatial resolution of 7.5 m. Brazil is a country with continental dimensions where different aerosols are generated, whether by natural or anthropogenic sources. The two systems mentioned above, SPU Lidar Station in São Paulo and DUSTER Lidar system in Natal, can measure different aerosols types.

Quality assurance and quality control programs developed by the European Aerosol Research Lidar Network (EARLINET) [8] are being implemented at the LALINET stations of São Paulo, Manaus, and Natal. This implementation intends to increase the capability to provide a reliable dataset in collaboration with three EARLINET stations (Bucharest, Granada, and Munich) in the framework of the project APEL (Assessment of atmospheric optical Properties during biomass burning Events and Long-range transport of desert dust) [9, 10]. The main objective is

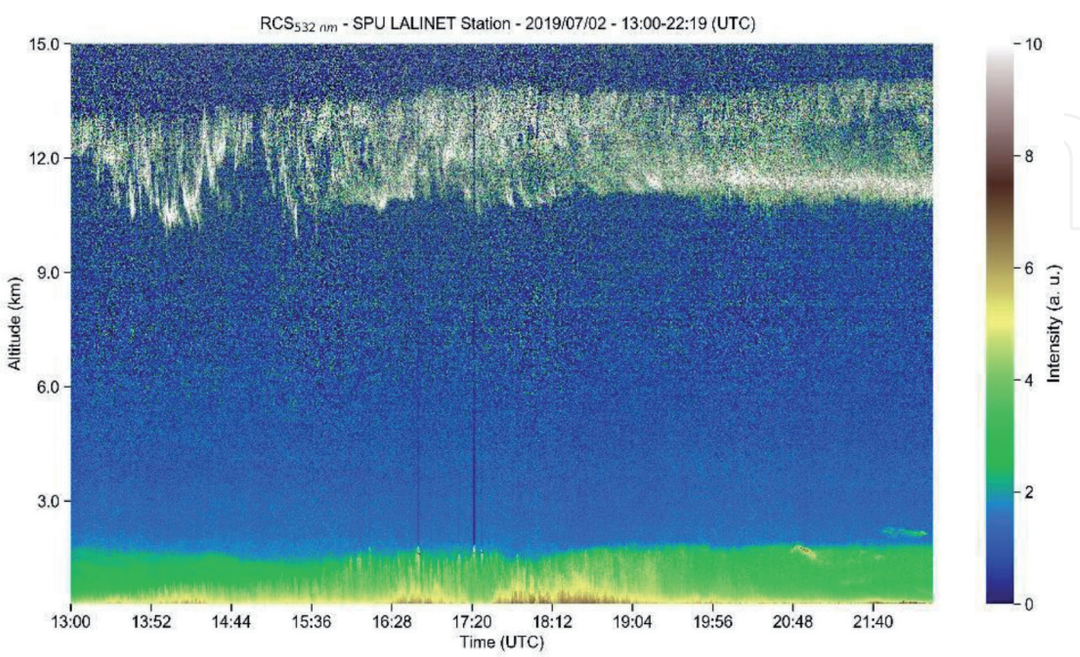

Figure 1.
Quick-look of the Lidar Range Corrected Signal (RCS) at 532 nm measured at SPU Lidar Station on 02 July 2019. The signal between 10 and 14 km indicates cirrus clouds.

to make the final data products from the two networks comparable and study the similarities and differences in aerosol loads, transport heights, types, and properties [11]. The evaluation will be done at the hardware and software levels. At the hardware level, the quality of the signals will be checked using the specific EARLINET procedures, and, at the software level, the LALINET data processing algorithms will be compared with the EARLINET Single Calculus Chain [12–14]. The last is a fully automatic evaluation process that can be used for virtually any lidar configuration and was validated for several EARLINET lidar stations, being a powerful tool that allows lidar stations to retrieve the aerosol backscatter and extinction profiles from the raw lidar data (**Figure 2**).

In Bolivia's case, the Laboratory for Atmospheric Physics of Universidad Mayor de San Andrés (LFA for its acronym in Spanish) is carrying out some studies related to urban aerosols and pollution monitoring in the metropolitan region of La Paz and El Alto. This region is one of the fastest-growing urban settlements in South America, with the particularity of being located in very complex terrain at a high altitude over the Andes. With a total population of around 1.8 million inhabitants is the second most populous urban area in Bolivia. La Paz city is located in a stepped valley, whose height starts at 3200 m a.s.l. (southern area), going up to 4000 m a.s.l. (in the north). The metropolitan area includes El Alto city (4100 m a.s.l), adjacent to the west's valley, and is extended over the Altiplano plateau. The valley has many basins that converge in the lower part of the city generating complex air fluxes.

An elastic lidar system was installed in the Science Campus of the Universidad Mayor de San Andrés (16.5333 S, 68.0667 W, 3420 m a.s.l.) in 2007 to study the boundary layer's behavior in this complex terrain. The lidar system was developed by improving an old system donated by the European Space Agency to the LFA and an essential collaboration of the Raman Lidar Laboratory of NASA's Goddard Space Flight Center. The instrument regularly worked for some years collecting data every Monday. These ancillary data were used for different short-term studies [15].

In 2011, this lidar acquired an additional relevance when a new Global Atmosphere Watch (GAW) station was set up near the metropolitan area at Mount

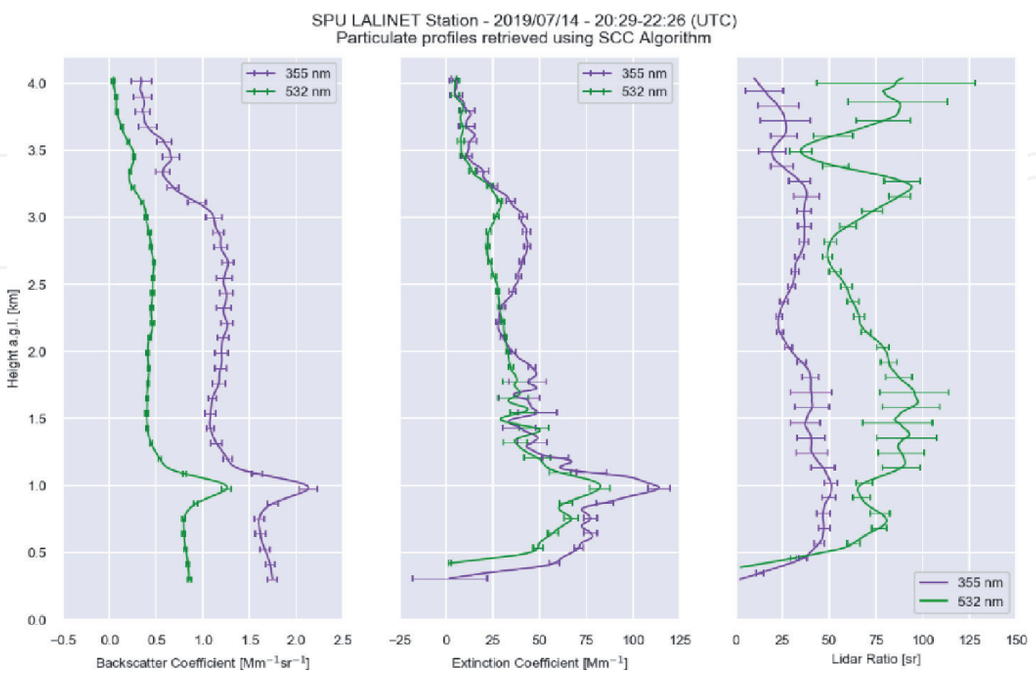

Figure 2.
Particle backscatter ($Mm^{-1}\ sr^{-1}$) and extinction (Mm^{-1}) coefficients and Lidar Ratio (sr), measured at SPU Lidar Station on 14 July 2019. Smoothed retrievals, obtained at 355 nm and 532 nm, using the Single Calculus Chain Algorithm.

Chacaltaya (16.3502 S, 68.1314 W, 5240 m a.s.l.). This station was set up to study aerosols' physical and chemical properties, measure atmospheric gas concentrations, study the aerosols injected into the free troposphere, besides the effect of aerosols deposition onto the Andean glaciers. In this sense, the main task of the lidar system was to help with the study of the air fluxes that go from the metropolitan area to the Chacaltaya GAW station and vice versa and the behavior of the local atmospheric boundary layer, especially in connection with atmospheric pollution in the urban area.

Besides, in 2018 and thanks to a collaboration of the Andalusian Institute for Earth System Research, Granada, Spain, a Lufft CHM 15 k ceilometer was installed in the northern part of La Paz city, closer to the Chacaltaya GAW station than the LFA. The goal was to characterize the boundary layer height's seasonal behavior through continuous measurements for at least one year. The Wavelet Covariance Transform (WCT) was used to estimate this behavior using both the ceilometer and the university campus's lidar. Although we gained knowledge about the local ABL's temporal behavior, it is clear that due to the complexity of topography in this region, extending this work's main conclusions is not straightforward. More measurements and modeling are needed for this purpose.

2. Urban aerosols and pollution monitoring

2.1 The atmospheric boundary layer

The Atmospheric Boundary Layer (ABL) is the lowest section of the troposphere and is directly affected by the surface, responding to surface forcing within a one-hour or less time scale. The ABL has turbulent properties and high variability in its daily cycle, and it is a fundamental parameter to several studies, e.g., air quality, numerical weather forecasting, climate modeling, and wind energy applications [16]. These characteristics, associated with the variations in the ABL stability, enable us to subdivide it into three main layers: The Convective Boundary Layer (CBL), the Stable Boundary Layer (SBL), and the Residual Layer (RL).

The ABL height (ABLH) is obtained from the vertical profile of some tracers like a potential temperature [17], vertical wind speed [18], relative humidity [19], and aerosols [11]. The radiosondes are the more traditional method to estimate the variation of some tracers indicated above and, consequently, estimate the ABLH. Nevertheless, in most regions, the radiosondes are launched only twice a day, which does not provide a detailed observation of the ABLH behavior. In this scenario, due to the lidar systems' high temporal and spatial resolution, the utilization of this kind of equipment to estimate the ABLH and other ABL properties had increased significantly in the last decade, mainly in South America [20–30].

Elastic lidar and ceilometers can estimate the ABLH from the characteristic reduction in the aerosol concentrations in the transition region between the Free Troposphere (FT) and ABL. **Figure 3** presents an example of the ABLH and its subdivisions, both estimated from elastic lidar data. Moreira et al. estimated the Urban ABLH to the city of São Paulo (Brazil), using elastic lidar data, from a method based on the curtain-plot of the Range Corrected Signal and Wavelet Covariance Transform (WCT), respectively [31, 32]. Both algorithms were validated by radiosonde data, resulting in high correlations during convective and clear sky conditions. Also, based on WCT, Niesperuza et al. estimated the ABLH to Medellín (Colombia), demonstrating the influence of the selections of the parameters in the Haar Wavelet performance [33]. Salvador et al. performed a comparison among the ABLH estimated from elastic lidar, SODAR, and Weather Research and

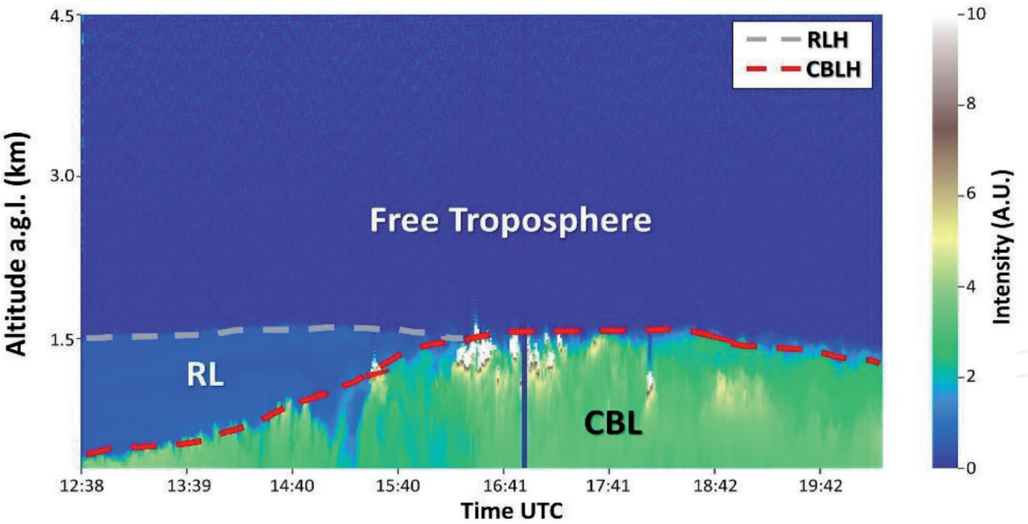

Figure 3.
ABL and its subdivisions. WCT and Gradient Methods, applied in elastic lidar data, estimated the CBLH and RLH. The aerosol profiles were measured at SPU Lidar Station on 03 August 2020.

Forecasting Model (WRF), finding a high positive correlation during the convective period [26]. Besides, elastic lidar data can also observe aerosol plumes' movement as the mixing level in the CBL region, from the skewness and kurtosis profiles. This method was applied in the city of São Paulo [34]. The methodology can be applied in studies about air quality providing a better observation about pollutant concentrations.

In comparison with elastic lidar, Doppler lidar provides more possibilities to identify the ABLH due to the capacity to obtain the wind speed profile, which can be applied as a tracer from its variance. Using Doppler Lidar data, Moreira et al. estimated the ABLH from the variance in the wind speed profile in São Paulo [24]. This method was compared with radiosonde data demonstrating a high correlation in CBL and SBL situations. The wind speed profile was used to detect low-level jets (LLJ). Then from the maximum of LLJ, the SBL height was estimated [25]. Marques et al. used the maximum variance in the Noise Ratio to estimate the ABLH. Such a result was compared with radiosonde data, reaching high correlations in stable and convective situations [28].

2.2 Retrievals from the LiDAR-CIBioFi station at Cali-Colombia

In Colombia (Cali), to detect the ABL altitude, lidar signals obtained from the LiDAR-CIBioFi station at Universidad del Valle are employed. The study site is georeferenced in **Figure 4**. The methodology employs an interplay between the Gradient [32, 33] and WCT [34] Methods, as described in detail in Ref. [27].

Statistical validation of the implemented instrumentation is performed to support the data quality by contrasting atmospheric profiles retrieved by radiosondes launched at the local international airport, a few kilometers away from our station. The maximum vertical gradient level of potential temperature is used to detect the ABL top (ABLT) by employing radiosonde profiles. A linear relationship between the daily ABLT evolution retrieved by the lidar station and the radiosonde profiles goes as follows: ABLLiDAR = 0.967 × ABLRadio - 0.022. It is statistically significant at the 95% confidence level and R^2 (consider the separation between the radiosonde launching site and the lidar station, see **Figure 4b**).

Once the data are validated, the ABLT levels are compared against the available local Particulate Matter (PM) concentration information. The correlations between

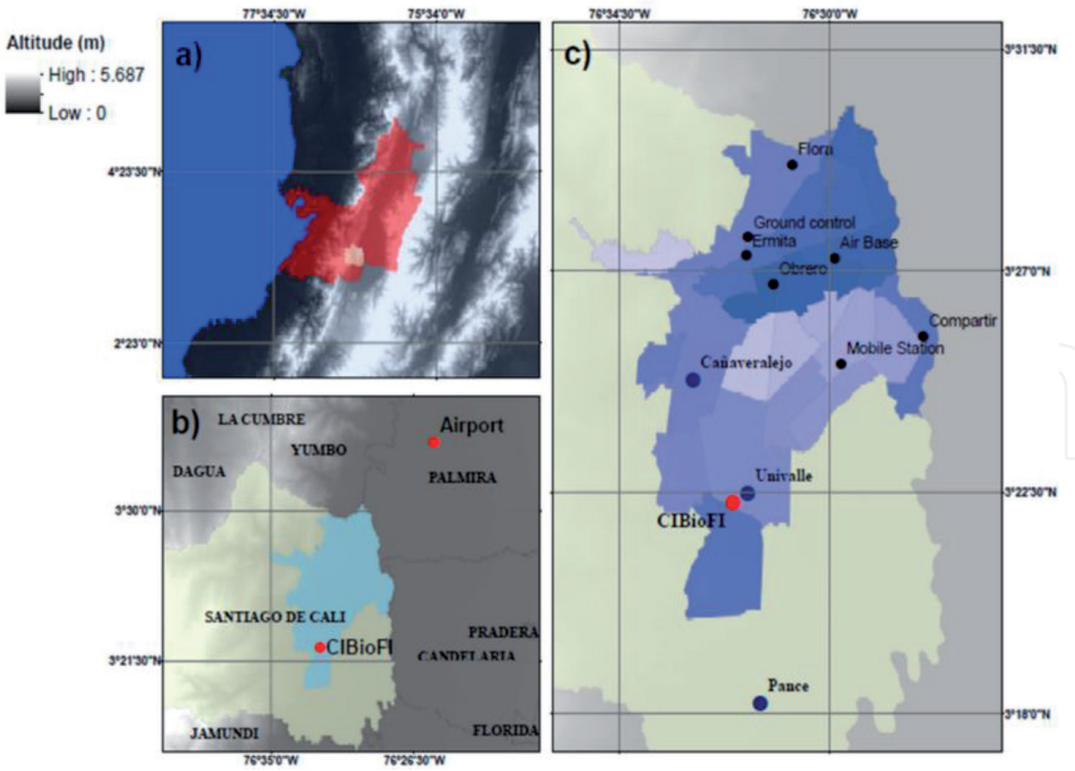

Figure 4.
(a) The location of Valle del Cauca county (the gray area) and the city of Cali (white area) in Colombia (altitude values according to the color scale). (b) The light color shape represents Cali's rural area. The blue region is linked to the city's urban area. The red dots mark the LiDAR-CIBioFi system's location at Universidad del Valle (UniValle) and the radiosonde station (at Cali's international airport). (c) Political and administrative division of Cali. The blue dots place the Air Quality Monitoring System (SVCA) ground stations of the local Administrative Department of Environmental Management (DAGMA).

daily ABLT evolution and PM concentration data from three representative city ground-stations (Cañaveralejo, Pance, and UniValle), shown in **Figure 4c**, are analyzed. A strong negative relationship for the Cañaveralejo station gives R^2 = 0.79, while the Pance station exhibits an unencouraging positive slope with a correlation coefficient R^2 = 0.13, meaning a PM concentration increase for higher ABLT values, with PM values above the World Health Organization limits. The UniValle station, located about 100 m away from the LiDAR-CIBioFi station, reveals a low negative correlation (R^2 = 0.20) for the ABLT evolution for all months, especially at the beginning of the wet season.

An innovative method for retrieving the ABL top from LiDAR signals was developed at the LiDAR-CIBioFi station. It consists of training a convolutional neural network (NN) in a supervised manner, driving it to learn how to retrieve this dynamical parameter on real, non-ideal conditions and, in a fully automated and unsupervised process [31]. The Wavelet Covariance Transform (WCT) is used as a labeling method for constructing the training data set and as a baseline method for comparison with the trained NN.

The dataset used for the model's training and tuning is composed of 15,000 signals extracted from daytime measurements taken during December 2018 and February 2019. The signals were labeled using WCT, with a custom search threshold for each one; this was done to ensure the labels' quality and, consequently, the neural network predictions [31].

It is expected that the corrected training of the model replicates the predictions of a signal-by-signal fine-tuned WCT but in a completely automated and non-supervised process. The convolutional neural network proposed for the ABLT detection is compared to WCT in a supervised variant (custom search threshold for

all time evolution) and unsupervised WCT (full signal as input during all time evolution) [31]. WCT was chosen as the labeling and comparison method for its ease of implementation and well-known robustness and performance, as for the past two decades, it has been used to measure the ABLT in numerous case studies [31].

On 14 August (**Figure 5a**), clouds around 4 km height, with some formations around 2 km, were detected, with the latter being very close to the boundary layer's height, thus posing a challenge for accurate ABLT detection. Besides, some cases of changes in density were detected after 14 h [31].

The first single lidar measured profile (**Figure 5b**), taken at about 12:30 h, exhibits a well-mixed layer, making it easy to discriminate between ABL and free troposphere. This condition allows a straightforward evaluation of the predictions: the NN gives very similar results to the supervised WCT (about 1.8 km), while the unsupervised WCT located the ABLT in a cloud formation above 4 km height [31]. In contrast, the second profile (**Figure 5c**), taken at 15:40 h, gives very different results for the supervised (sup.) WCT, the unsupervised WCT, and the NN. The supervised WCT located the ABLT at 500 m, below the expected result.

The unsupervised WCT placed the result at around 4 km, in a cloud formation pattern, while the NN located the ABLT about 2.6 km, following its actual behavior [31]. The temporal evolution of the LiDAR measurement profiles of **Figure 5** clarifies that the unsupervised WCT detection locates the boundary layer position at cloud formation height, erroneously placing the ABLT in most cases [31]. The supervised WCT shows ABLT detection problems, severely underestimating ABLT for cases of proximity to clouds (see, e.g., around 12 h), and in cases of residual layers (e.g., after 14 h). Despite the drawbacks of supervised WCT and unsupervised WCT, **Figure 5** clearly shows that our convolutional NN estimation of ABLT is more resilient to nearby clouds than WCT [31].

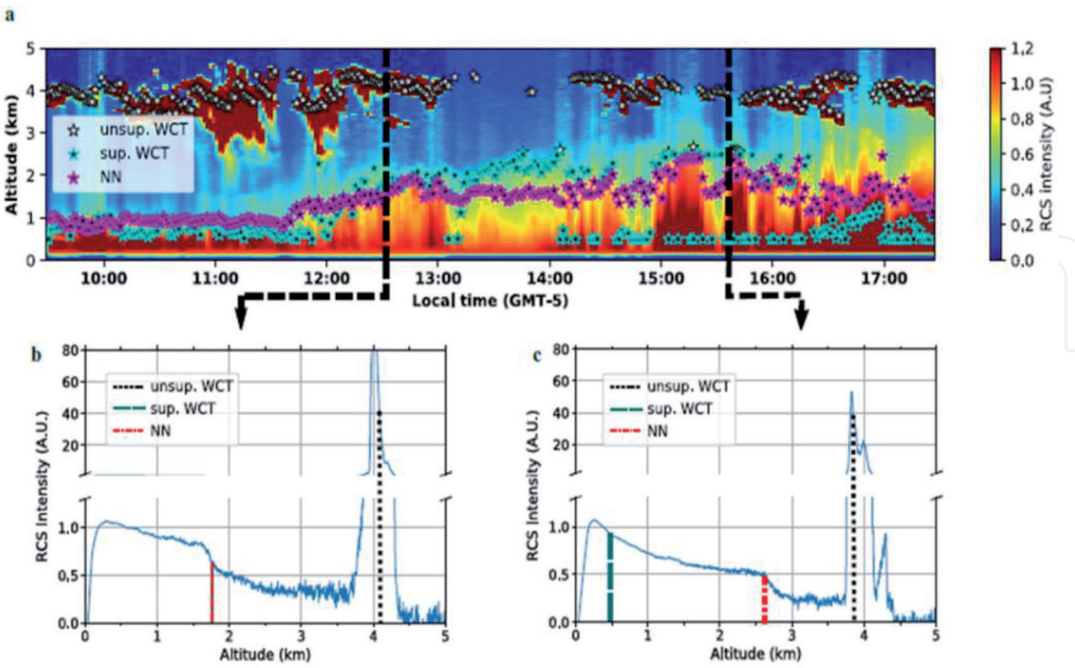

Figure 5.
Lidar retrievals for 14 August 2019 [30]. (a) Temporal evolution of the ABL, and (b), (c) Two selected single profiles. They point out different scenarios treated with our method: the measurements exhibit b Profile 1 (12:30 h), a well-mixed layer where NN and sup. WCT values are very similar, and c, Profile 2 (15:40 h), shows conditions where the NN estimation differs from supervised and unsupervised WCT values; the latter profile exhibits an extended ABL a height of about 2.6 km for the NN prediction. The intensity of the signals is given in arbitrary units (a. u.) [31].

The SVCA is the local Air Quality Monitoring System, a governmental policy for continuously monitoring air quality and assessing the pollutants trend. This air quality network provides information in the medium and long term to support developing strategies to attend to the air pollution effects from a holistic view. This network is composed of nine ground stations distributed, as shown in **Figure 4**. There are six stations to measure PM_{10} concentration and four stations for $PM_{2.5}$ concentration measurements. These stations count with automatic analyzers technology for monitoring aerosols and gases such as ozone, carbon dioxide, and others. Employing the raw data retrieved by these stations, the local Administrative Department of Environmental Management (DAGMA) makes monthly and annual reports, which can be found [31] at http://www.cali.gov.co/dagma.

Hourly raw data from three ground base stations that belong to the SVCA network were used to analyze the daily behavior of PM_{10} and $PM_{2.5}$. Due to its proximity to the LiDAR-CIBioFi station, Cañaveralejo, Pance, and UniValle stations have been picked. Specifically, the UniValle station is about 100 m away from the LiDAR-CIBioFi, and for a direct intercomparison with ABL altitude is a primary source of data. The data retrieved from these ground stations are significant since they are the only available aerosols data source that features Cali to support environmental public policy reinforcement; these are meant to control day-by-day vehicular fleet restrictions and industrial emissions.

One way to assess the impact of PM concentration on public health and radiative forcing is to study its response according to the ABL vertical and horizontal dynamics. We account for PM_{10} and $PM_{2.5}$ concentrations retrieved by the automatic analyzers and the vertical atmospheric profiles from LiDAR-CIBioFi. The correlations for the PM as a function of the ABL altitude retrieved by the LiDAR system, the vertical response of PM for each station, according to the ABL daily evolution during July, August, September, and October 2018, are analyzed. The daily data are used as a first step to identify PM daily behavior within the ABL.

The hypothesis to understand the relationship between PM and ABL is that the aerosol's mass volume has an inverse behavior to the ABLT evolution. **Figure 6** shows how daily data from Cañaveralejo station (red dots) already comply with this hypothesis: PM_{10} concentration decreases with the ABL height; this behavior is a continuous trend for each of the four covered months, regardless of the temperature and solar radiation transition along the day. Especially in the mornings, the Cañaveralejo station reports the maximum concentration amongst the three stations, with values not above the local 24-hour limit.

Regarding Pance (green dots) and UniValle (blue crosses) stations, the regressions exhibit odd behavior, particularly during July and August 2018: **Figure 6a** and **b** show that Pance's PM_{10} concentration dangerously grows with increasing ABL height, a situation of concern since this means that the population remains exposed to high concentrations within a large air volume mass in the ABL. Since we do not have additional information about the emission source, we postulate that Pance high concentrations could be attributed to tropical forests' haze. Nevertheless, it is necessary to warn on this behavior and spot possible emission sources, and identify such aerosols' optical properties.

The Pance and Cañaveralejo stations were chosen due to their proximity to the LiDAR-CIBioFi station, but their locations correspond to a different landscape, and the ABLT dynamics could be very different from that of UniValle's. Since UniValle station is located about 100 m away from the LiDAR-CIBioFi station (and within the same university campus), it is a direct source for PM data comparison/analysis against ABLT dynamics; it is, however, necessary to keep in mind that UniValle station only makes measurements of fine ($PM_{2.5}$) particles concentration. Even though UniValle station shows $PM_{2.5}$ values well below those of PM_{10} Pance and

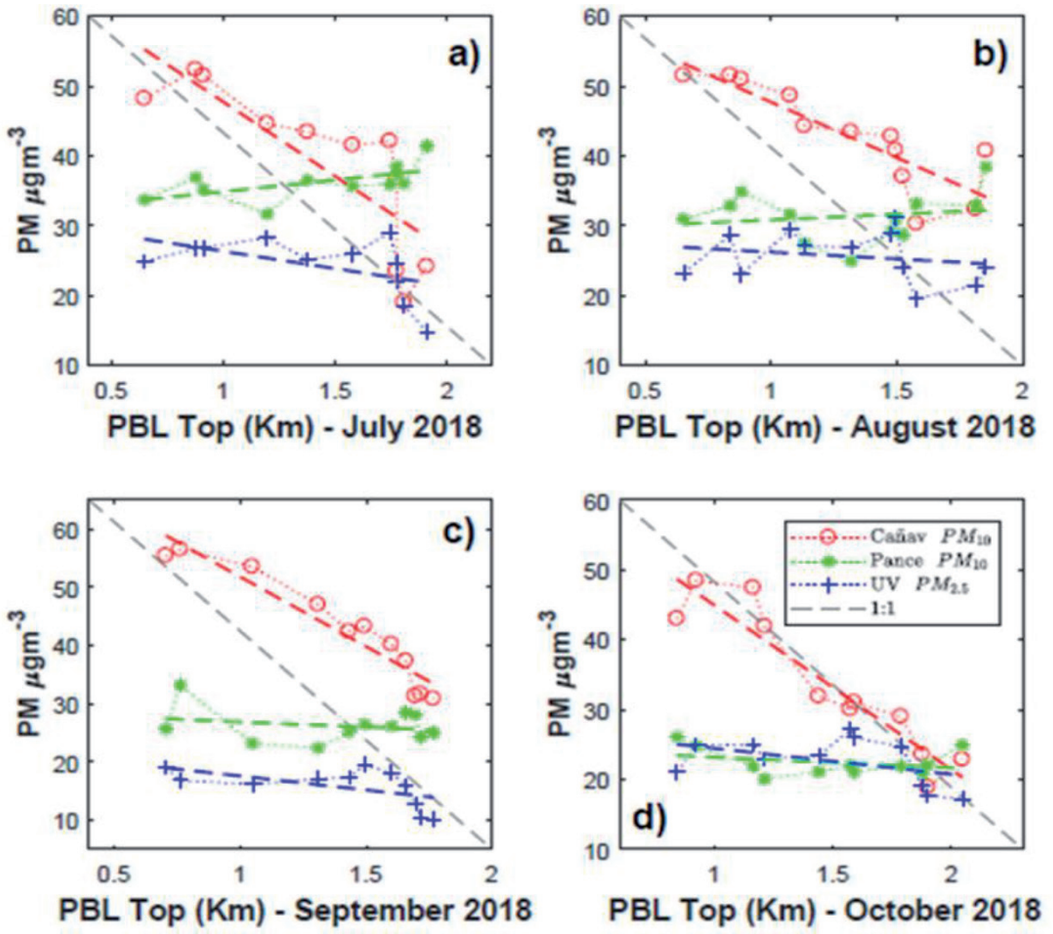

Figure 6.
(a) Linear regression between PM (μg m^{-3}) concentration and ABLT (or PBL top-planetary boundary layer top) altitude retrieved by LiDAR-CIBioFi in July 2018. (b), (c), and (d) denote the same as in (a) except for the month of data collected (August, September, and October 2018, respectively).

Cañaveralejo stations during July, August, and September, during October 2018, Pance and UniValle registered very similar values for $PM_{2.5}$ and PM_{10} against the ABL height; this means a high worrying indicator of fine ($PM_{2.5}$) particles concentration at UniValle. The linear regression between UniValle and Pance stations and the ABL height shows similar behavior. Thus, $PM_{2.5}$ concentration values are kept almost constant during the whole day and ABL height evolution. These fine particles' size allows them to stay longer in the atmosphere, explaining the regression line trend.

All data for each station in **Figure 6** and corresponding regressions were organized chronologically. Hence, regarding air quality, unquestionably, the most critical report is that for UniValle station due to the size of measured particles and the worrying linear regression balance with the ABLT daily evolution. The reported concentration levels are slightly above the local annual threshold and the World Health Organization (WHO) 24-hour PM limits.

To summarize, the ABLT results obtained at the LiDAR-CIBioFi station were compared against three PM SVCA ground-stations (Pance, Cañaveralejo, and UniValle) to analyze the behavior of the correlation with PM concentration near the LiDAR station. The Cañaveralejo station that carries out PM_{10} measurements shows an inversely proportional relationship with the ABLT, indicating that the population is not overexposed to PM_{10} concentration as higher ABLT values are reached. On the other hand, PM_{10} and $PM_{2.5}$ concentrations retrieved by Pance and UniValle stations show a different relationship with ABLT. Unexpectedly, the linear correlation slopes for each one of these stations were quite close to zero. The slope's mean value for

Pance station was 1.67, reporting positive values for July and August, which means that PM_{10} concentrations increased with increasing ABLT, a word of warning due to a possible negative impact on public health. On the other hand, the slope's mean value for UniValle ($PM_{2.5}$) station was −3.85, with negative monthly mean values.

3. Detection of biomass burning events

Wildfires generate large amounts of suspended particles in the atmosphere and increase the levels of carbon monoxide. The presence of these particles reduces both visibility and solar radiation reaching the Earth's surface. Besides, they act as cloud condensation nuclei, modifying the climate and the air composition and being harmful to human health [35]. On 8 November 2019, a dense feather of smoke was detached from Australia's coasts due to the intense fires that affected the region. These smoke layers were dragged by the winds to South America, entering Argentine territory on 14 November and remaining in suspension until the next day. In the particular case of the fires in Australia, a large amount of soot not only affected the entire surrounding region, devastating forests, and wildlife: the effects were seen around the planet, with measurements of the transport of aerosols at thousands of kilometers from the emission sources. An immediate effect of the accumulated soot from such a biomass burning was the alteration of river courses and the drinking water production in Eastern Australia [36].

The Australian fires started in September 2019 and intensified in November, given the drought conditions that affected the region. It was the second warmest summer registered, having a rainfall regime below the Australian summer average [36]. These major fires produced dense smoke plumes, detected by the Suomi NPP (National Polar-orbiting Partnership) VIIRS (Visible Infrared Imaging Radiometer Suite) satellites. The images are presented in **Figures 7** and **8** for 8 November, and in **Figures 9** and **10**, for 9 November. The figures show Australia's east coast, the most affected area. **Figures 7** and **9** show the Earth's surface's natural-looking satellite images, called True Color RGB images (I1-M4-M3). Meteorological clouds can be distinguished in white and smoke layers in translucent gray tones. **Figures 8** and **10** show another combination of spectral bands (M11-I2-I1), which allows observing, in shades of blue, the smoke plumes and, in reddish shades, the scars left on the surface of the Earth by fires (burned surface) [37]. These smoke plumes crossed the Pacific Ocean, reaching the American continent and Argentine territory in mid-November 2019.

Measurements from sensors onboard satellites and ground-based platforms were used to analyze the November biomass burning aerosols intrusion event from Australia. Within the satellite measurements, the data from the OMPS sensor (Ozone Mapping Profiler Suite) [38, 39] onboard the Suomi NPP satellite were analyzed for the study of the space–time variability of the Aerosol Index (AI Aerosol Index). AOD (Aerosol Optical Depth) measurements at 550 nm were retrieved from the MODIS (Moderate Resolution Imaging Spectroradiometer) instrument onboard the TERRA satellite [40, 41]. Additionally, the total columnar CO (carbon monoxide) content and the AI were sensed by the TROPOMI (TROPOspheric Monitoring Instrument) instrument onboard the Sentinel-5P satellite [42, 43]. AI is a qualitative index that indicates aerosol's presence at the higher layers of the atmosphere, absorbing or reflecting UV radiation. The main types of aerosols detected with this index are desert dust, biomass burning, and volcanic ash plumes. An advantage of AI is that it can be calculated for clear and (partially) cloudy ground pixels.

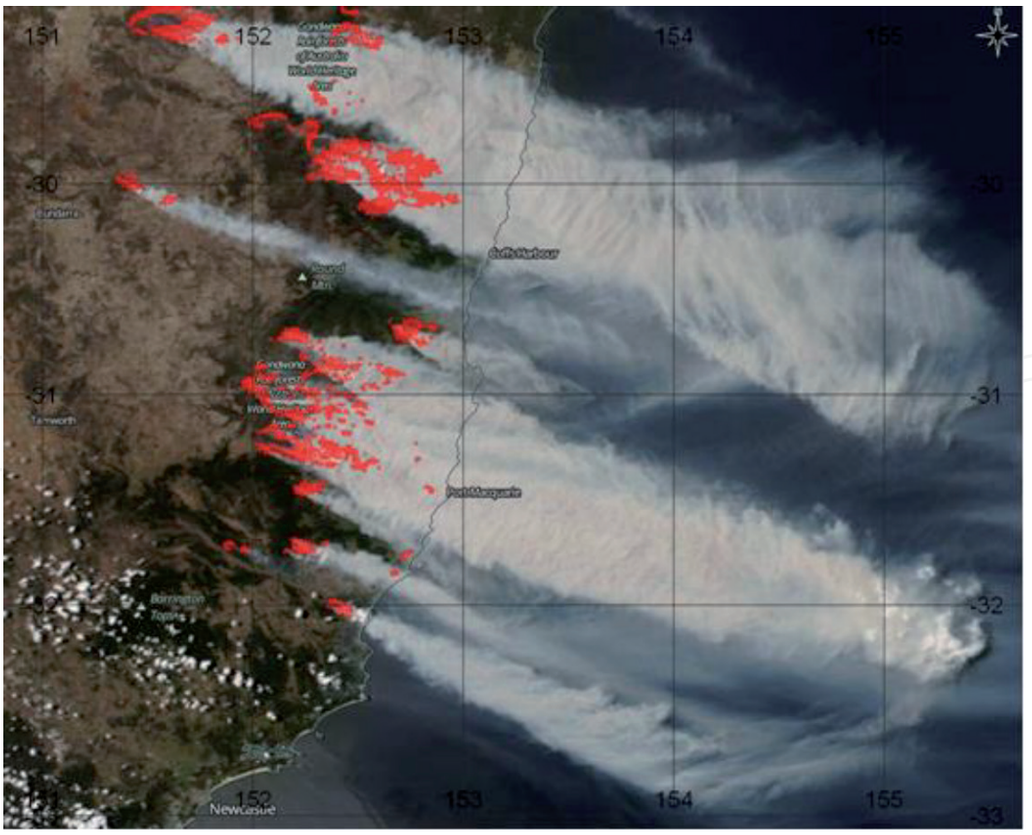

Figure 7.
Satellite image of Australia's east coast from 8 November 2019. VIIRS - Suomi NPP sensor (combination: I1-M4-M3).

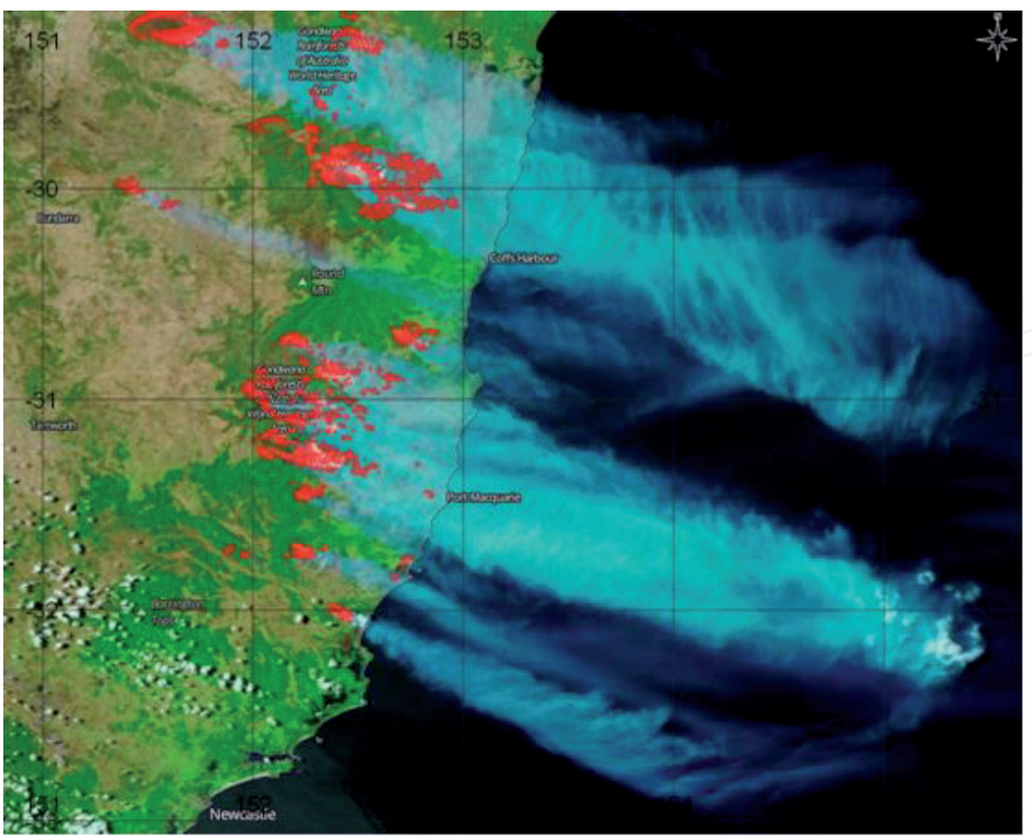

Figure 8.
Satellite image of Australia's east coast from 8 November 2019. VIIRS - Suomi NPP sensor (combination: M11-I2-I1).

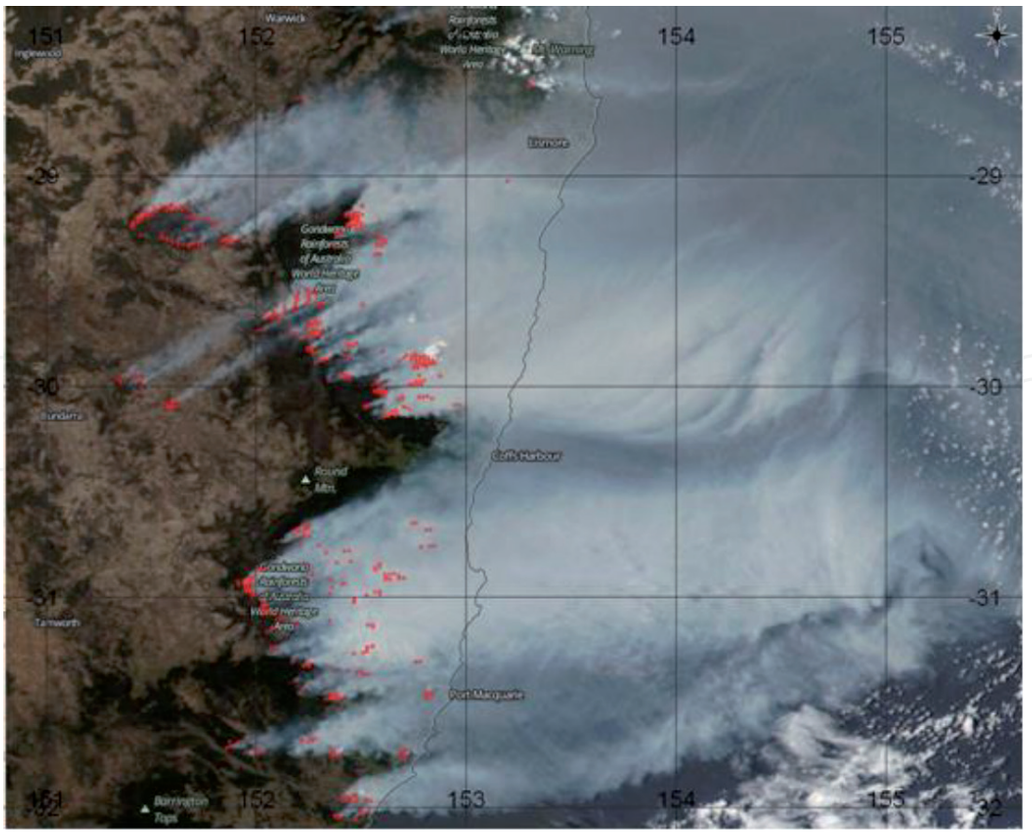

Figure 9.
Satellite image of Australia's east coast from 9 November 2019. VIIRS - Suomi NPP sensor (combination: I1-M4-M3).

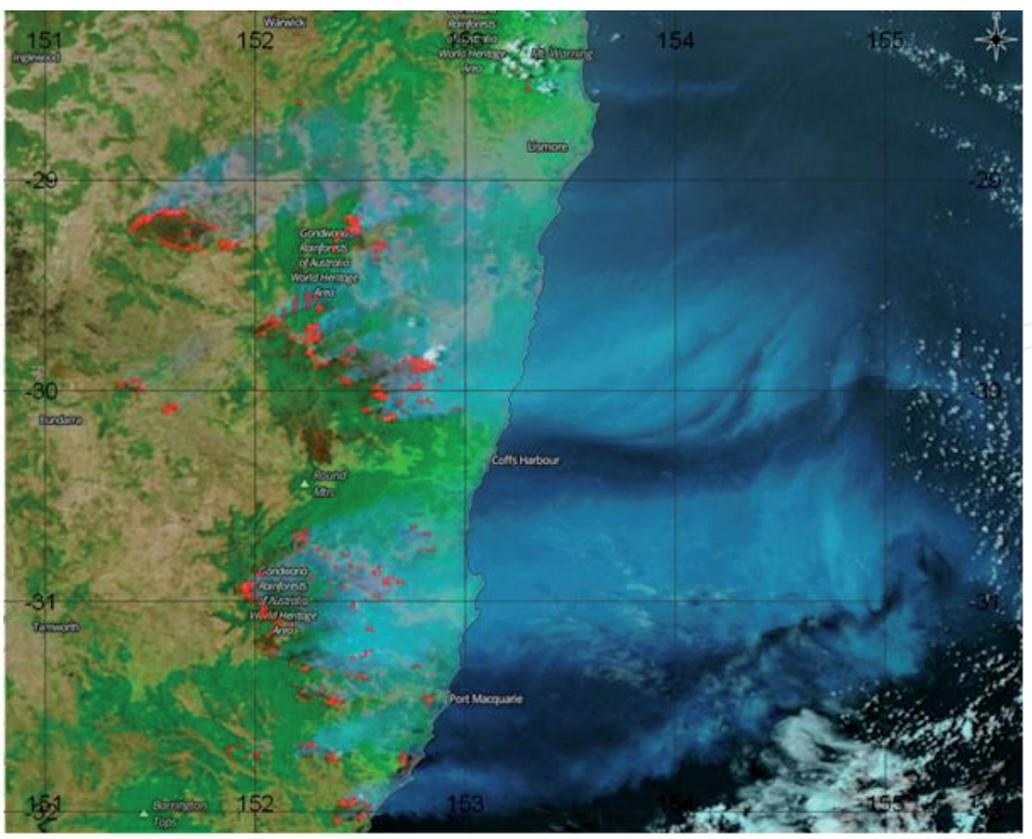

Figure 10.
Satellite image of Australia's east coast from 9 November 2019. VIIRS - Suomi NPP sensor (combination: M11-I2-I1).

The ground-based aerosol optical depth (AOD) data is obtained from the AERONET/NASA sun photometer network measurements at Buenos Aires, CEILPA-BA (34.555 W, 58.506 S, 26 m), Córdoba, and Pilar (31.667 W, 63.883 S, 333 m) stations, at Level 1.5 (data where the clouds have been extracted automatically) [44, 45].

The AOD is the aerosol vertical column integrated extinction at a given wavelength. This dimensionless quantity indicates how much aerosols attenuate the solar radiation as it passes through the atmosphere. Another value, the Ångström coefficient (or exponent), shows the AOD spectral dependence, and it is related to the root mean square distribution of the aerosol radii. It is calculated as the slope of the linear fit of the spectral AOD in a particular wavelength interval in a log–log scale graph. By relating the AOD at 440 nm and the Ångström coefficient, it is possible to classify the aerosol type using the classification table of Reference [46].

Measurements from the lidar instrument installed at CITEDEF were analyzed to determine the height of the aerosol layers. The normalized aerosol backscattering coefficient was calculated at 532 nm [47–49]. This system allows measuring the atmosphere's profiles from a few meters to several kilometers, exceeding the tropopause height up to the lower stratosphere. **Table 1** summarizes the variables analyzed, the sensors, and the platform employed.

Figure 11 shows the AI's space–time evolution measured by the OMPS sensor from 8 to 13 November 2019. The images show how a high AI value (greater than 5) smoke plume emerges from Australia's coasts on day 8 November 2019. This plume advances over the Pacific Ocean and reaches the coast of South America on 13 November 2019.

On 14 November 2019, the Australian smoke arrived over Argentine territory for the first time, through Neuquén province and covering the country's entire central region. **Figure 12** shows the AI coverage map (OMPS), indicating aerosols' presence throughout the area.

Figure 13 shows the TROPOMI sensor AI measurement for 14 November. The AI retrieved from OMPS and TROPOMI show similar values, around 1, in almost the entire territory and, in particular, values between 2 and 3, in the province of Entre Ríos. Both overlapping measurements are plotted in **Figure 14** to compare the AI measurements coverages with the two sensors. The TROPOMI measurement is taken as the basis, and the polygon (red outline) from the OMPS AI coverage is superimposed. It can be seen that the presence of aerosols in the upper layers of the atmosphere is the same for both sensors. It is known that biomass burning is one of the primary sources of CO release to the atmosphere. **Figure 15** shows the regional

Platform	Sensor	Variable
Satellite Suomi NPP	OMPS	AI
Satellite Sentinel 5p	TROPOMI	CO AI
Satellite TERRA	MODIS	AOD (550 nm) Ångström coefficient
Ground-based	LIDAR	Aerosol backscatter
Ground-based	Sun Photometer	AOD (440 nm) Ångström coefficient

Table 1.
Instruments and variables used to analyze the November biomass burning aerosols intrusion event.

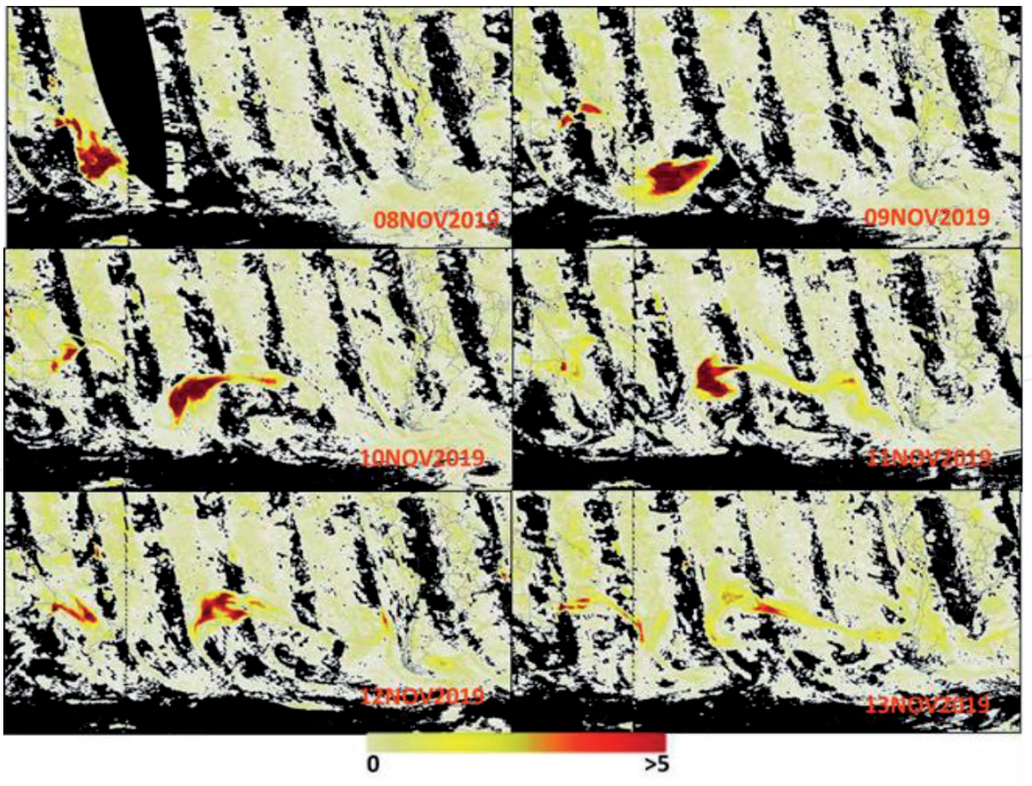

Figure 11.
Spatial–temporal evolution of the smoke plume through the OMPS sensor analysis of the Aerosol Index (AI), from 8 to 13 November 2019.

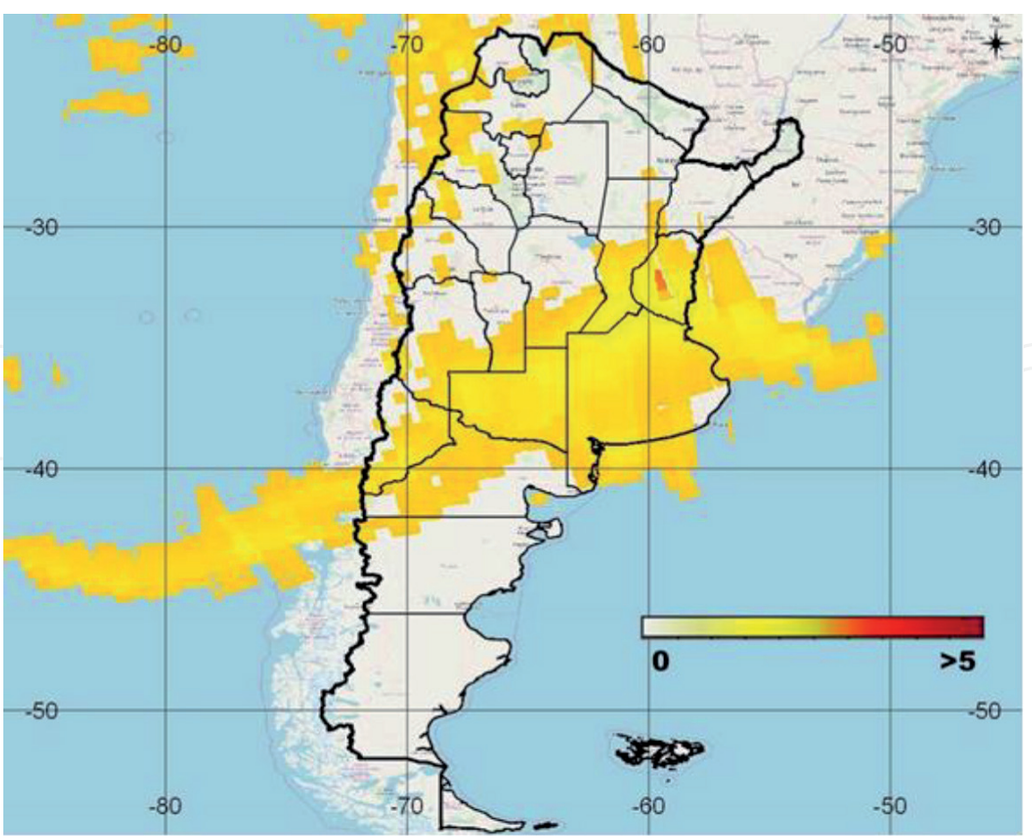

Figure 12.
Aerosol Index (AI), calculated by the OMPS sensor measurements for 14 November 2019.

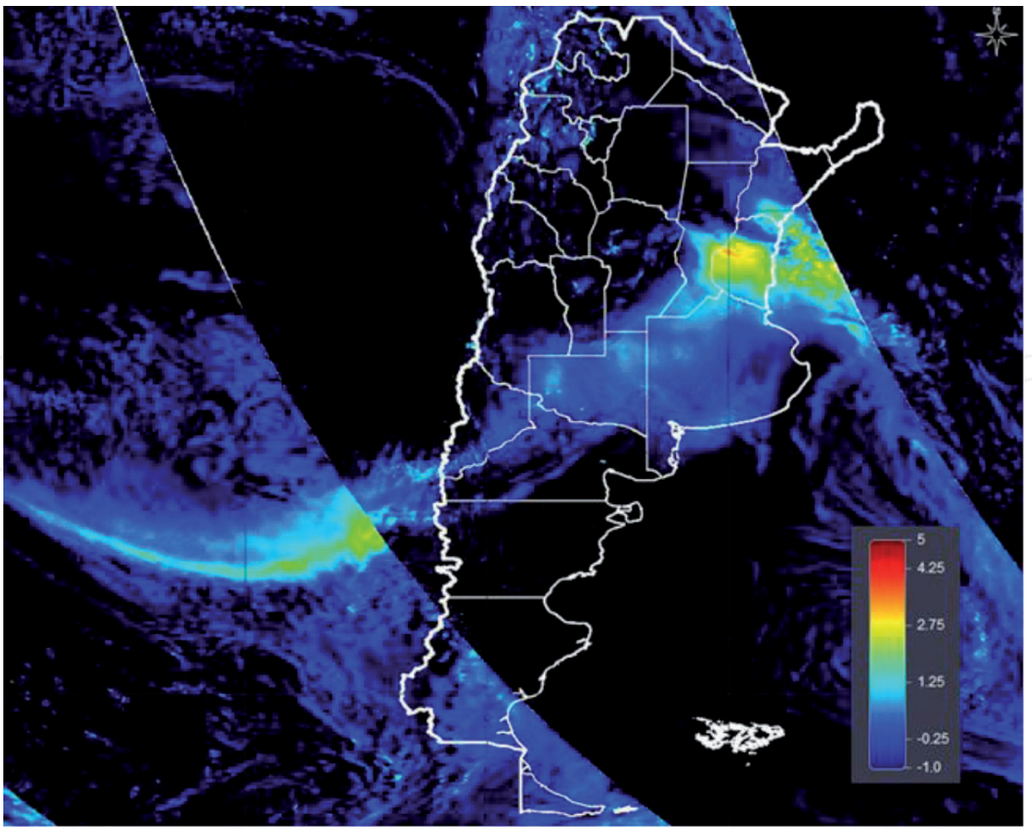

Figure 13.
Aerosol Index (AI), measured with the TROPOMI sensor for 14 November 2019.

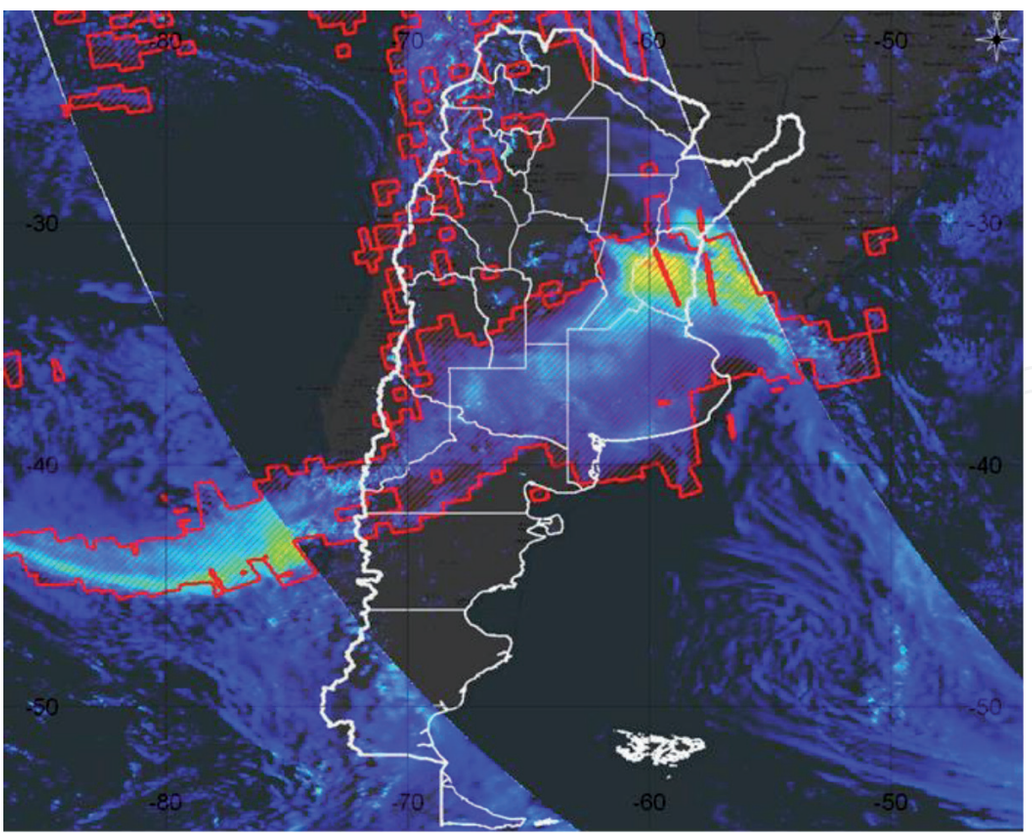

Figure 14.
Comparison of the Aerosol Index (AI) coverages, calculated with the TROPOMI sensor (in color palette) and the OMPS sensor (polygon in red), for 14 November 2019.

total columnar abundance of CO measured by the TROPOMI instrument [50]. The values observed throughout the region are not high.

A slight increase of CO measurements was observed in the same area where AI values were high, as shown in **Figure 16**, where the CO measurement overlaps the AI coverage (OMPS - red polygon). CO measurements reached a maximum of 0.04 mol/m^2 over the province of Entre Ríos.

A slight increase of CO measurements was observed in the same area where AI values were high, as shown in **Figure 16**, where the CO measurement overlaps the AI coverage (OMPS - red polygon). CO measurements reached a maximum of 0.04 mol/m^2 over the province of Entre Ríos.

Another interesting measurement to analyze the aerosols' presence is the AOD, which indicates at which level the aerosols prevent the sunlight from passing through the atmosphere. Aerosols scatter and absorb sunlight, resulting in reduced visibility. An AOD of less than 0.1 is characteristic of a clean atmosphere, with a very low number of suspended particles and maximum visibility. The AOD increases due to the increase of suspended particles, and this causes visibility loss.

Figure 17 shows the AOD measurement at 550 nm from the MODIS - TERRA sensor for 14 November 2019. Maximum values of 0.6 are observed in the southern part of the province of Entre Ríos. Values about 0.3 in the vicinity of the City of Buenos Aires and 0.2 in the vicinity of the City of Córdoba are also observed.

This satellite measurement can be contrasted with the AERONET/NASA sun photometer measurements available at Buenos Aires and Córdoba. **Figure 18** shows the AOD temporal evolution at 440 nm for 14 and 15 November 2019 for the Buenos Aires station and 15 November 2019 for the Córdoba station. At both stations, the values are higher than 0.1 along the two days.

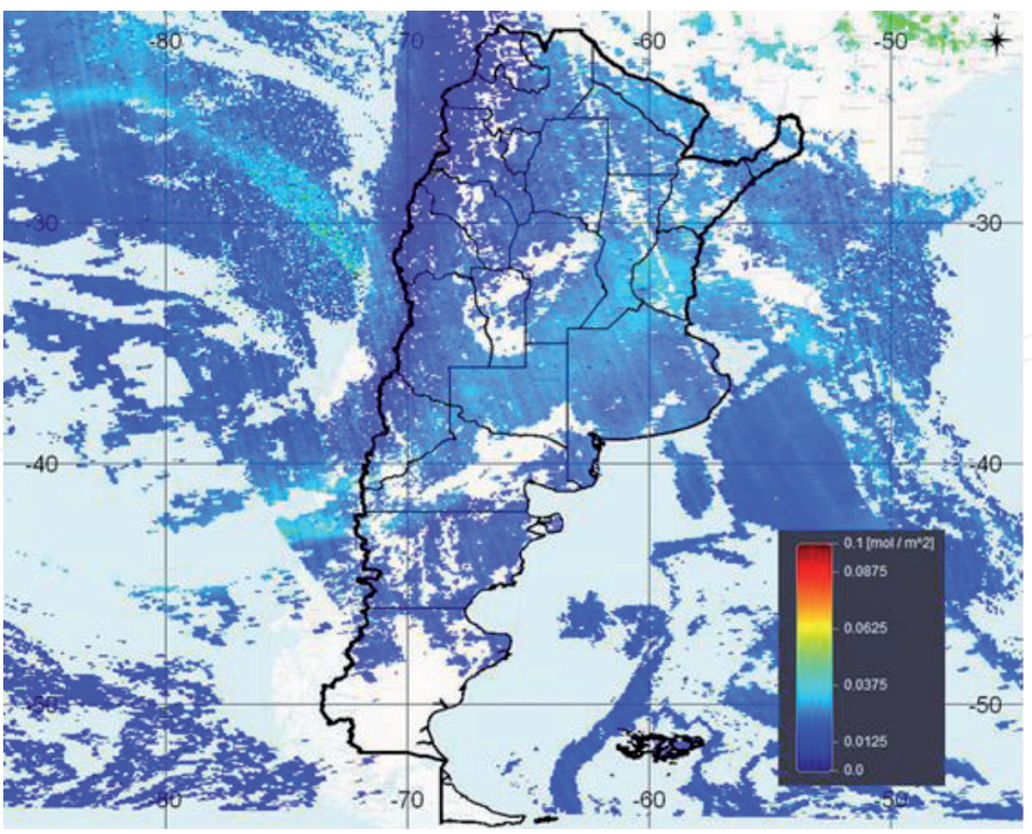

Figure 15.
CO in the total column from TROPOMI-Sentinel-5P for 14 November 2019.

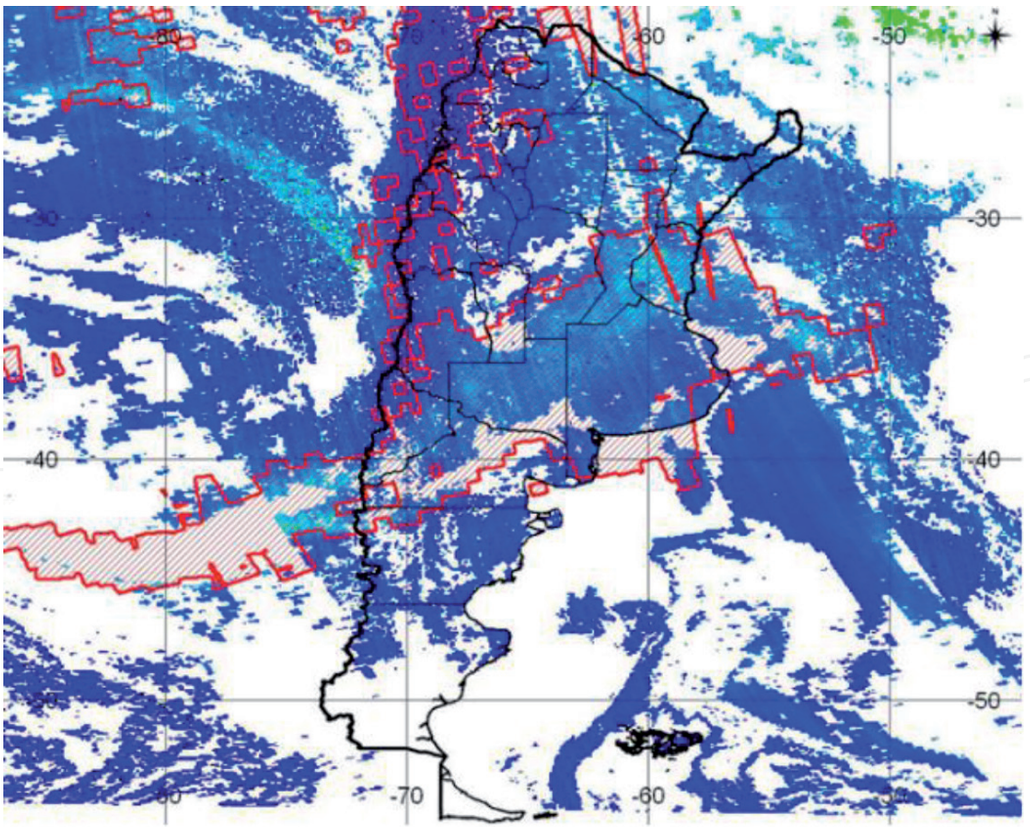

Figure 16.
CO in the total column from TROPOMI-Sentinel-5P and the coverage of the AI (OMPS - red polygon).

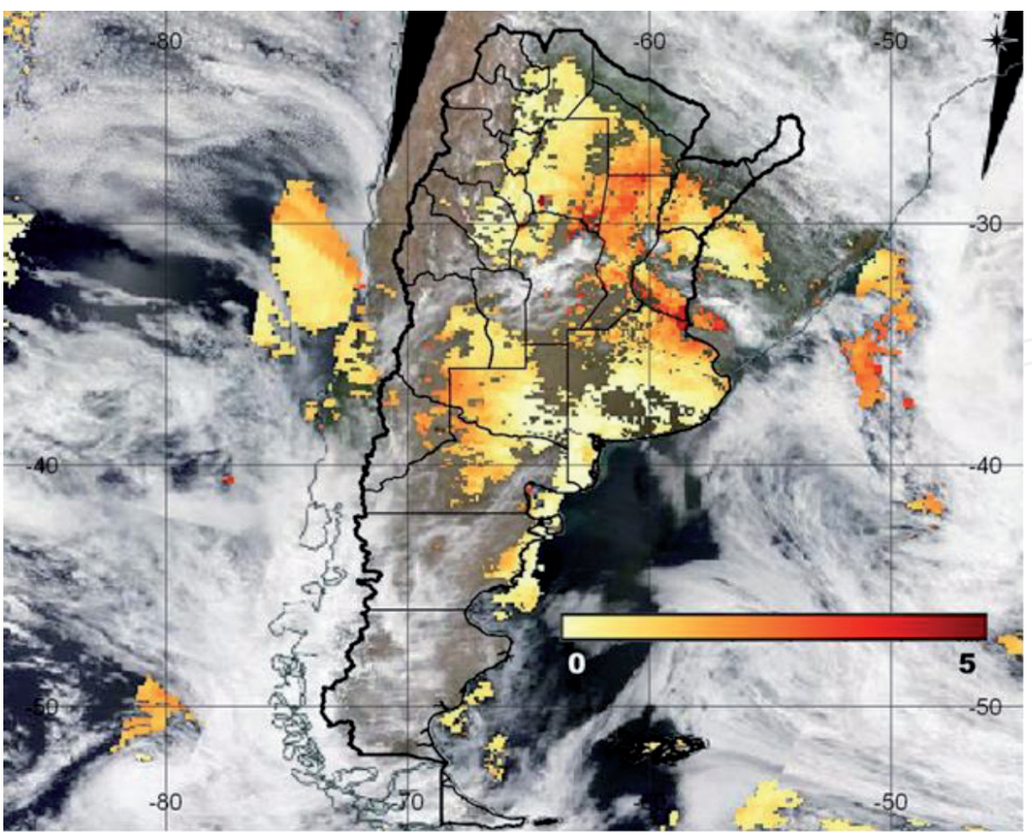

Figure 17.
AOD at 550 nm from MODIS-TERRA for 14 November 2019 (logarithmic scale).

The Ångström coefficient calculation can be used to provide additional information related to the size of the aerosols. The higher this coefficient is, the smaller the particle size. Values less than 1 suggest the domain of coarse particles (e.g., dust), and values greater than 1 suggest the domain of fine particles (e.g., smoke). **Figure 19** shows the Ångström coefficient from MODIS-TERRA product, where maximum values of 1.8 are observed in the southern part of Entre Ríos (in light blue), and 1.1 in the surroundings of Buenos Aires and south of Santa Fe (in green).

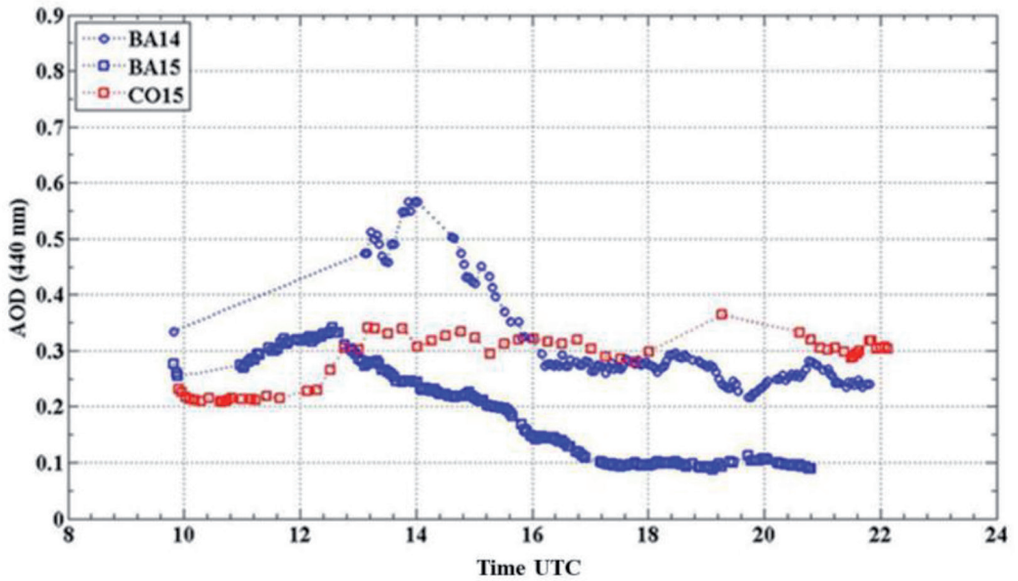

Figure 18.
Temporal evolution of the AOD at 440 nm during 14 and 15 November 2019 (BA: CEILAP-BA station (blue); CO: Pilar station (red)).

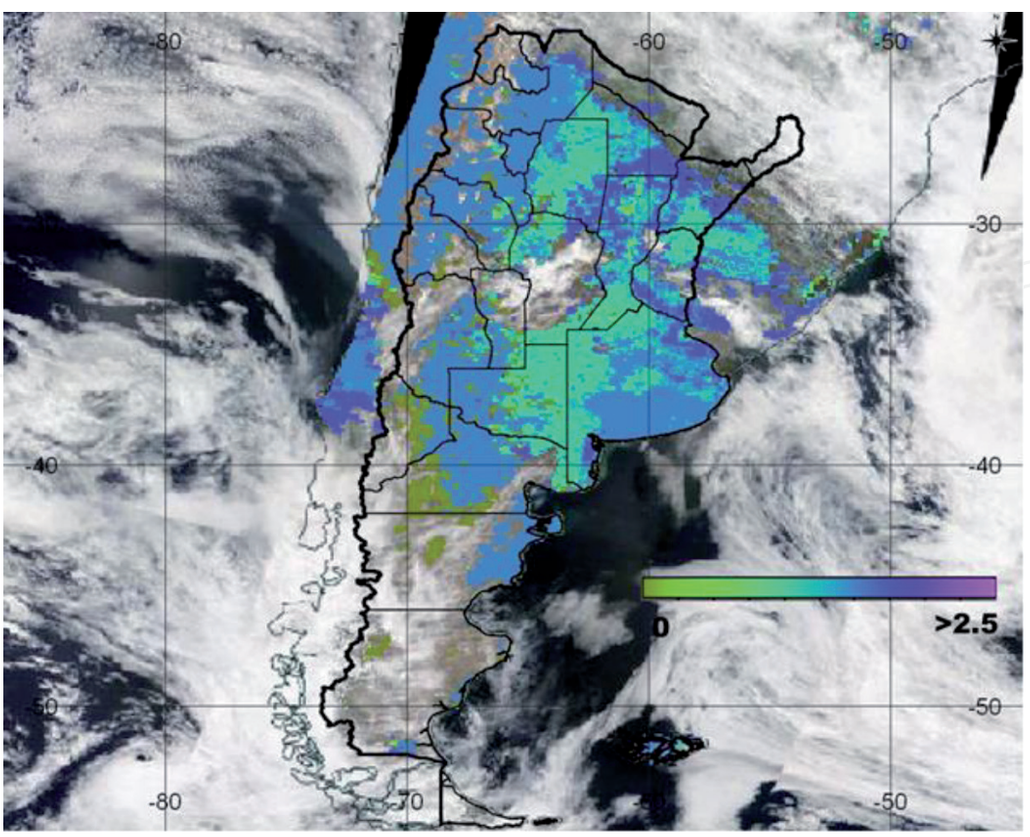

Figure 19.
Ångström coefficient (Blue) of MODIS-TERRA for 14 November 2019.

The Ångström coefficient was calculated from the AERONET/NASA sun photometers' AOD data at 870, 670, 500, and 440 nm. **Figure 20** shows the AOD at 440 nm versus the calculated Ångström coefficient. This style of graphs allows classifying the type of aerosols suspended in the atmosphere. From such an analysis, it can be extracted that most of the particles are originated from biomass burning, therefore being of the types Biomass Burning and Contaminated Continental, according to the classification table in Ref. [46].

Measurements with the lidar system made it possible to determine the aerosol layers' heights over the City of Buenos Aires. **Figures 21** and **22** show the normalized aerosol backscattering spatial–temporal evolution at 532 nm. On the horizontal axis is UTC's time (Local Time is UTC-3 h); on the vertical axis is the height in kilometers (the tropopause is about 13 km). The color palette shows the intensity of the signal. The blue color represents a clean, molecular atmosphere (without suspended particles), and the red color indicates particulate material. For both days, numerous well-defined layers of aerosols were observed above the atmospheric boundary layer at various heights and with different intensities, up to 13 km.

This work analyzed one event of the arrival of smoke plumes from Australia's intense fires to the Argentinean territory in November 2019. The study determined that, during that period, the AOD values were about 0.25, on average, and the Ångström coefficients were about 1.2. The aerosol layers were found above the atmospheric boundary layer, between 2 km and 13 km of altitude, in the vicinity of the City of Buenos Aires. The CO values were slightly increased without presenting significant risk values for human health. The importance of conducting this type of study is to show that in such aerosols transport events, particles can be transported for hundreds of kilometers from their origin and affect the climate, air quality, and visibility of other areas very distant from the emission source. Satellite measurements, in combination with sun photometers and lidar systems measurements, have allowed an essential synergy for the detection and spatial–temporal monitoring of the smoke columns that, generated thousands of kilometers away, arrived in Argentine territory. Together, these measurements help understand wildfires' environmental impacts in short and long time series, as they provide relevant data for climate and particle dispersion models [51].

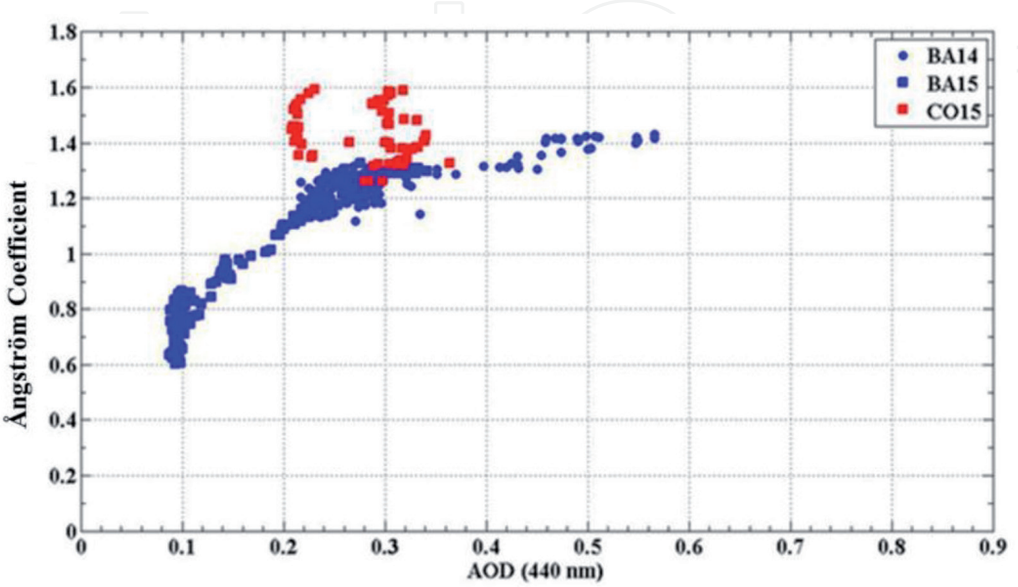

Figure 20.
Ångström coefficient versus AOD (440 nm) for 14 and 15 November 2019 (BA: CEILAP-BA station (blue); CO: Pilar station (red)).

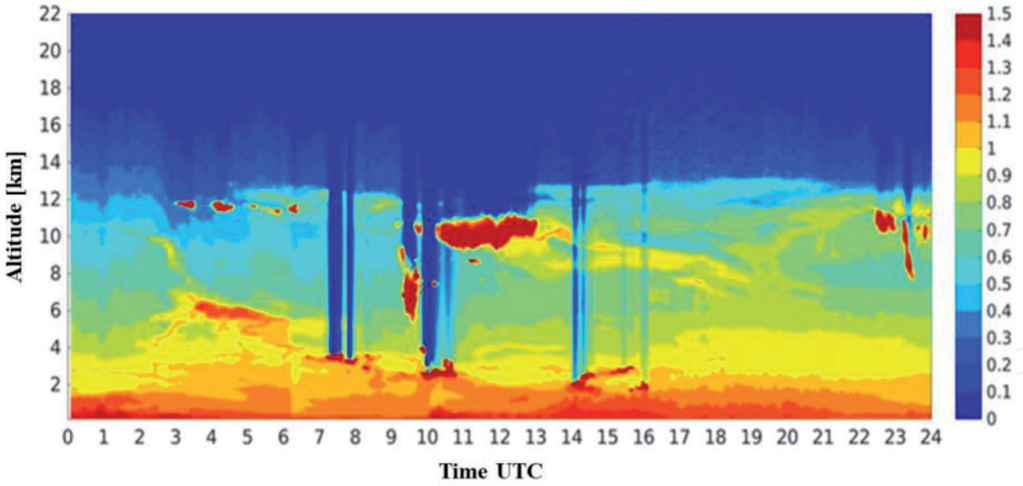

Figure 21.
Spatial–temporal evolution of the normalized aerosols backscattering at 532 nm for 14 November 2019.

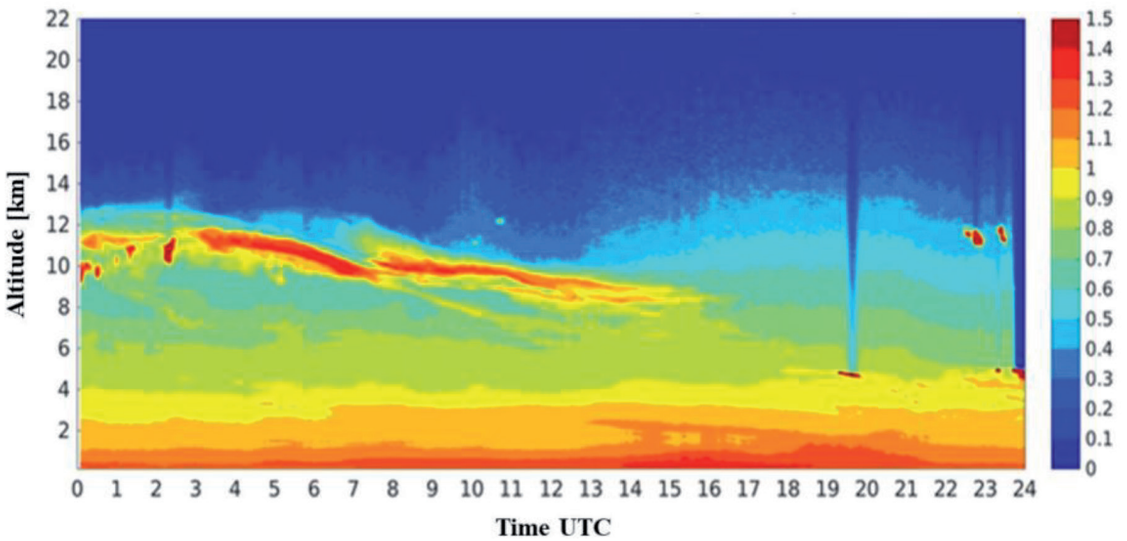

Figure 22.
Spatial–temporal evolution of the normalized aerosols backscattering at 532 nm for 15 November 2019.

4. Dust transport

The long-range transport of desert dust has an essential impact on the atmospheric radiative balance, with a global impact on climate, air quality, and human health [52, 53]. It is estimated that between 1 and 2 billion tons of dust are transported from Sahara each year through the atmosphere [54, 55].

Knowledge of the transport mechanisms of dust aerosols from the Sahara Desert to the South American continent can help understand its impact on the balance of nutrients in the Amazon basin [56, 57] and its nutrients deposition in the equatorial Atlantic [58]. Dust transport from the Sahara over the Atlantic Ocean can reach distances greater than 5000 km from its origin and is more intense during December, January and February at 5 N, and during June, July, and August at 20 N latitude. During the boreal winter, desert aerosols are transported across the Atlantic towards the northeast coast of South America, and in the summer, they can reach the Caribbean Sea [59].

The most favorable periods to observe the presence of Saharan dust with a lidar in the atmosphere of the city of Natal (located about 5 S) are in December, January, and February. In this period, Oliveira et al. [60] found the mineral dust

predominance occurred during February, followed by December, January, and March in 2018. Research with lidar on aerosols in the Natal atmosphere focuses on the long-range transport of mineral dust and also smoke from biomass burning from the African continent, occurring under the strong influence of the trade winds, during austral summer, when the Intertropical Convergence Zone (ITCZ) is positioned further to the south [61, 62]. In a case study on 09 February 2018 (Reference [60]), Oliveira et al. show that aerosol plumes were identified below 4000 m altitude.

Landulfo et al. were the first to identify an aerosol plume with a lidar, at 3000 m altitude in Natal's atmosphere, on 01 June 2016 [63]. Direct measurement of the Sun and radiances of the sky with a CIMEL solar photometer may also be used to identify the measured dust aerosol, as in Ref. [60]. Similar aerosol identification studies were carried out [57, 61, 62, 64, 65], showing that African dust's transatlantic transport reaches the Caribbean. Episodes of mineral dust particles transported from Africa to the Amazon between January and April were also observed [66].

The DUSTER Lidar system started operating in 2016 with operational data collection campaigns called MOnitoring aerosol LOng-range Transportation OVer Natal (MOLOTOV) Zero (March 2016 to July 2016.), MOLOTOV I (December 2016 to mid-February 2017), MOLOTOV II (January and February 2018), and APEL (Assessment of Atmospheric Optical Properties During Biomass Burning Events and Long-Range Transport of Desert Dust) (November and December 2017), at the Federal University of Rio Grande do Norte (UFRN), in Natal.

Also, during the campaigns MOLOTOV Zero and MOLOTOV I, eighteen cirrus cloud profiles were analyzed (7 during MOLOTOV Zero and 11 from MOLOTOV I). Part of the research was conducted to calibrate the DUSTER system, applying the Δ90° method [67]. The main physical parameters of cirrus clouds obtained from lidar data were their thickness, base height, top height, and linear particle depolarization (δp) [68, 69]. The determination of parameters such as base height and top height was calculated from the analysis of the depolarization profiles obtained for each data interval. Data from radiosondes launched by the Natal airport (about 7 km from the DUSTER system) were used to obtain the average cirrus temperature. The average depolarization value for cirrus clouds during the MOLOTOV Zero campaign was $\delta p(\text{cirrus}) = 0.43 \pm 0.15$ with an average base height of 14.23 km and an average top height of 15.53 km [70]. The average temperature of cirrus during this campaign was −69.23°C. The average thickness of the cirrus found was 1.30 km. For the MOLOTOV I campaign, the average value was $\delta p(\text{cirrus}) = 0.49 \pm 0.13$ with the average base height equal to 12.96 km and the average top height equal to 14.44 km. The average thickness found was 1.48 km. The average cirrus temperature found for this campaign was −62.06°C [70].

5. Cloud studies

Clouds play an important role in Earth's radiation budget as they reflect incoming solar radiation and absorb outgoing thermal radiation emitted from the surface, the atmosphere, and other clouds [71]. In tropical regions, Cirrus clouds are omnipresent [72] and hence affect the radiation balance significantly because of their sizable horizontal extent (hundreds to thousands of km) and long lifetime (hours to days). Cirrus optical properties, altitude, vertical and horizontal coverage control, radiative forcing, and detailed measurements are of absolute value [73, 74].

Studies reporting cirrus properties over tropical South America used to be scarce, with most studies based on in-frequent satellite observations [72, 75]. For obtaining detailed geometrical and microphysical properties of Cirrus clouds,

especially the sub-visible type, ground-based lidars are indispensable. For this reason, many lidar groups around the world have used such measurements to obtain and report these characteristics in mid-latitudes [74] and tropical regions [76]. A similar effort is being made in South America, mostly under the auspices of LALINET. Here we review studies from five LALINET stations (Cuba, Manaus, Natal, São Paulo, and Punta Arenas), and we also discuss results from Reference [77], who report on measurements in Buenos Aires. It is compiled a set of statistics for optical and geometrical properties of cirrus occurring in this side of the world, summarized in **Table 2**.

The first studies were performed in Cuba by the lidar group in Camagüey using 6-years (1993 to 1998) elastic lidar data [78]. The lidar measurements were performed for detecting aerosols in the stratosphere, and hence were conducted mostly on clear nights to the naked eye, thus introducing a bias in the cloud measurements towards subvisual cirrus clouds. Indeed, from 131 clouds measured, only 8% were thick (COD >0.3), 67% were thin (0.03 < COD <0.3) and 25% were sub-visual (COD <0.03). Sub-visual and thin cirrus have an average cloud top and base at 14.1 and 11.6 km, respectively, with thick clouds occurring at slightly lower altitudes. The authors estimated the respective optical depths to be 0.50 ± 0.27, 0.07 ± 0.05, and 0.02 ± 0.01, but these are an upper limit as they were calculated assuming a lidar ratio (LR) of 10 sr, which we now know is too low.

In a follow-up study, Barja and Antuña performed radiative transfer simulations (GFDL model, Freidenreich and Ramaswamy, 1999) of the impact of cirrus clouds on solar radiation (SW) [83]. They have found that the daily mean value of SW cirrus radiative forcing (CRF_{SW}) has an average value of −9.1 W m^{-2} at the top of the atmosphere (TOA) and −5.6 W m^{-2} at the surface (SFC). There is a linear relation between CRF_{SW} and COD, with a slope of - 30 W m^{-2}/COD at TOA. The local radiative heating effect where the cirrus is found ranged from 0.35 to 1.24 K day^{-1}, with an average of 0.63 K day^{-1}. These results were the first to show that tropical cirrus radiative impact on Earth's energy balance is essential.

In the Amazon region, Gouveia et al. used continuous measurements (July 2011 to June 2012) at the Manaus station [1] to retrieve the optical and geometrical properties of cirrus clouds during day and night [79]. The cirrus frequency of occurrence was about 88% during the wet season and not lower than 50% during the dry season, with a mean column optical depth of 0.25 ± 0.46. The cloud top and base heights, as well as cloud thickness and cloud optical depth, were, respectively, 14.3 ± 1.9 (std) km, 12.9 ± 2.2 km, 1.4 ± 1.1 km, and 0.25 ± 0.46, similar to the values reported in Cuba. These clouds have a significant radiative impact with such a high frequency of occurrence and altitude over the dark-pristine Amazon forest (albedo about 0.12).

Gouveia then used these measured optical depths and vertical profiles of the cirrus extinction coefficient [84], at 5-min and 200 m resolutions, and calculated the cirrus radiative forcing (CRF) with libRadtran [85]. Cirrus in the Amazon region produced a net CRF at TOA and SFC of +15.3 and − 3.7 W m^{-2}, respectively, much more intense than predicted for 3 European sites (+0.9, +1, and + 1.7 W m^{-2} at TOA) [74, 86]. Optically thicker cirrus, in general, have more prominent net CRF, with instantaneous CRF that could reach extremes up (down) to +140 (−65) W m^{-2} for the night (day) time [85]. Together, the vertical profiles with total COD >0.3 were responsible for about 72% (62%) of the TOA (BOA) net CRF, which means that a large fraction of the CRF is generated by optically thin cirrus (COD <0.3) that are harder to detect by radars and passive instruments on board of satellites [86]. A definite daily cycle of the optical depth was found and shows a minimum about local noon and a maximum in the late afternoon (~16 h LT), associated with the diurnal precipitation cycle. This results in a mean instantaneous TOA (SFC)

Loc.	Camagüey, Cuba	Manaus, Brazil	Natal, Brazil	São Paulo, Brazil	B. Aires, Argentina	P. Arenas, Chile
Ref.	[78]	[79]	[80]	[81]	[77]	[82]
Lat.	21 N	3 S	6 S	23 S	35 S	53 S
Period	1993–1998	2011–2012	Jan-Feb 2017–2018	Jun-Jul 2007	2001–2005	2016–2018
λ (nm)	532	355	532	532	532	532
Freq.	41%	74%	67%	54%	—	45%
Top	14.1 ± 1.4	14.3 ± 1.9	13.4 ± 1.6	12.4 ± 0.6	11.8	10.8 ± 2.2
Base	11.6 ± 1.5	12.9 ± 2.2	11.5 ± 1.9	10.2 ± 0.7	9.6	9.0 ± 2.4
COD	0.50 ± 0.27	0.35 ± 0.55	—	0.27 ± 0.22	—	0.25 ± 0.32
LR (sr)	10 (fixed)	23.6 ± 8.1	—	26 ± 12	—	—

Table 2.
Cirrus clouds' properties were measured by different LALINET stations, from north to south, during the last 15 years. Columns indicate latitude (deg) of the station, period of study and wavelength, frequency of occurrence, cirrus layer average top and base altitudes, column cloud optical depth (COD), and lidar ratio (LR).

net CRF ranging from +1.7 (−23) W m^{-2} in the afternoon to +47 (+3.1) W m^{-2} at night [86]. The cirrus clouds produced an average in-cloud heating rate ranging between −1 K day^{-1} to +2 K day^{-1} vertical profile from 8 to 18 km (in-cloud), but with instantaneous values that can reach values higher than 10 K day^{-1} for portions of the cloud with high ice water content [86].

The DUSTER Lidar station at Natal, Brazil, is the most recent addition to the network. Cirrus measurements started only recently, and Santos reports on measurements during January–February (pre-rainy season) of 2017 and 2018 [80]. A total number of 35 clouds were studied and showed cirrus up to 16 km. These clouds are lower than those in Manaus and were never observed above the tropopause at 17–18 km. The reason is the less vigorous convection in this coastal site, which resembles an oceanic precipitation regime. The frequency of occurrence and average cloud top altitude was 74% (57%) and 13.9 km (12.3 km) in 2017 (2018), respectively. In situ data obtained by radiosondes (9.5 km away) for selected case studies showed an increase of the relative humidity in the layer where the lidar identified the cirrus clouds, from around 10–20% below/above the cloud to around 40–55% in the cloud altitude region.

Cirrus clouds over São Paulo, in the subtropics of South America, were studied by Larroza [81]. She analyzed 34 days, from June to July 2007, using the methodology described in Ref. [87]. The cirrus frequency of occurrence was 54%. The vertical distribution of cloud tops showed peaks at 9.6, 10.6, 12.3, and 13.9 km, with an average of 12.4 km. These cirri were optically thinner (0.27) and occurred at lower altitudes (cloud top 12.4 km) than their tropical counterpart but had a similar lidar ratio of about 26 sr. The clouds observed were either produced by the passage of cold fronts or transported from the tropics or mid-latitudes.

Going into the mid-latitudes, Lakkis et al. used data from a lidar system in Buenos Aires, Argentina, that was not part of LALINET [77]. They studied 60 diurnal cirrus clouds from 2001 to 2005. Unlike the tropics and sub-tropics, cirrus tops were only found very close to the tropopause (~380 m), with cloud tops at 11.8 ± 0.86 and bases at 9.6 ± 0.9 km. Unfortunately, the low statistics did not allow the calculation of a frequency of occurrence, nor did the authors report values of optical depth or lidar ratios. The southernmost LALINET station is at Punta Arenas, Chile (53°S, 71°W), a sub-Antarctic region. Lidar cirrus measurements there began in October 2016 and continue to the present. A preliminary result of cirrus clouds' geometric characteristics in the region, over two years (from 2016 to 2018), shows that the cirrus' mean base height is 9.0 ± 2.4 km and the mean top height is 10.8 ± 2.2 km. In the same site in November 2018, the Leipzig Aerosol and Cloud Remote Observations System (LACROS) [88] was deployed by the Leibniz Institute for Tropospheric Research (TROPOS) in collaboration with the University of Magallanes (UMAG) for the field experiment DACAPO - PESO (Dynamics, Aerosol, Cloud And Precipitation Observations in the Pristine Environment of the Southern Ocean). Cirrus clouds measurements are being performed with a Raman polarization lidar that will allow the calculation of LR and COD at multiple wavelengths, which will be reported in a future study.

There has been a great effort to study cirrus clouds in South America, with measurements taking place from 1993 to today, and from 21 N to 53 S. **Table 3** summarizes the main characteristics, and we can see how the cirrus altitude changes from the Tropical (high, 14.3 km) to the sub-Antarctic regions (low 10.8 km). The frequency of occurrence also becomes smaller, reducing from 74% in Manaus to 45% in Punta Arenas. Deep convection, prevalent in the tropics and sub-tropics, pushes the tropopause upward and creates optically and physically thick cirrus clouds from the anvil's detrainment. From the subtropics towards the polar regions, convection is limited by the lack of surface heating, and the mixing of tropospheric air depends on

		CRF_{SW}	CRF_{LW}	CRF_{NET}
Barja and Antuña Camagüey, Cuba	**SFC**	−5.6	—	—
	TOA	−9.1	—	—
Gouveia Manaus, Brazil	**SFC**	−5.0 ± 0.4	1.25 ± 0.04	−3.7 ± 0.2
	TOA	−5.7 ± 0.5	21.0 ± 0.6	15.3 ± 0.4

Table 3.
Cirrus Clouds radiative forcing (W m^{-2}) over Cuba [83] and the central Amazon forest [79] calculated by radiative transfer simulations based on ground-based lidar measurements.

uplift by frontal systems. This does not reach high altitudes, and the primary cirrus production mechanism will be the large-scale lifting of water vapor, rendering physically and optically thinner clouds. Lidars can directly observe the optical depth, and **Table 3** shows that it also becomes smaller, decreasing from 0.35 in Manaus to 0.25 in Punta Arenas. Unfortunately, there are not enough LR estimations to allow for a comparison. They were calculated only for Manaus and São Paulo, and the results are in close agreement, indicating similar crystal habits and formation mechanisms, as expected. Similar relation of the cirrus features and latitude was first reported by Cordoba-Jabonero et al. using data from the LALINET subtropical station of São Paulo and ground-based lidar located in Belgrano Antarctic Station [88].

Another aspect of this LALINET effort is the diversity in the methods and the timespan of the different studies, limiting our ability for a more in-depth comparison. The combination of the Klett and transmittance methods, as described by Larroza [87] and Gouveia et al. [79], can be applied to elastic data from any of the LALINET lidars, providing COD and LR with high temporal resolution (e.g., 5-min), during both day and night. The use of radiative transfer models to calculate the cirrus' radiative impact could also be performed for all stations doing cirrus measurements. It would be essential to homogenize cirrus clouds' analysis throughout the network groups, even by sharing analysis algorithms. Moreover, it should be emphasized that these critical analyses could be automatized and performed unattended on a unique central server. These facts highlight the importance of establishing systematic data sharing in the context of LALINET and GALION.

6. Conclusions

Tropospheric lidars can provide impressive results: aerosol studies related to volcanic eruptions, tropospheric systems, biomass burning, and dust transport (both into and out of the continent) were conducted over the past 15 years. Pollutant dispersion studies in large cities of South America employing PBL dynamics, conducted in different sites, and with specific conditions, greatly aid local air quality authorities. More recently, studies on clouds and their impact on radiative transfer have been carried out. Given the geographical location of the lidar sites, essential comparisons can be carried on along a wide longitudinal interval, and tropospheric-stratospheric circulation experiments can be performed, as well as their climatological interpretation.

Acknowledgements

The authors are thankful to the Brazilian Agencies National Council for Scientific and Technological Development (CNPq), Coordination for the

Improvement of Higher Education Personnel (CAPES), São Paulo Research Foundation (FAPESP), Brazilian Agricultural Research Corporation (EMBRAPA), and National Institute of Amazonian Research (INPA) LBA Central Office in Manaus. The authors also thank the NASA/AERONET teams, Japan International Cooperation Agency (JICA), the Argentine Agencies National Scientific and Technical Research Council (CONICET), National Agency for the Promotion of Research, Technological Development and Innovation (ANPCyT), the Argentine National Defense University (UNDEF), UNDEFI and PID-UTN Projects, the Ministry of Defense of Argentina, and the French National Centre for Scientific Research (CNRS). Also, to all NASA's technical personnel, the Argentine Institute of Scientific and Technical Research for Defense (CITEDEF), and the Argentine National Meteorological Service (SMN), who have kept the solar photometers in operation, and especially to Raúl D'Elia. The authors wish to acknowledge the entire NASA CALIPSO and MODIS (AQUA/TERRA) teams, the NOAA Air Resources Laboratory, for providing the HYSPLIT transport and dispersion model and the READY website, ESA/EOM projects teams, the Suomi NPP (National Polar-orbiting Partnership) Mission teams, and the Sentinel 5-P TROPOMI team. The authors also acknowledge the financial support from CIBioFi, the Colombian Science, Technology, and Innovation Fund-General Royalties System (Fondo CTeI-Sistema General de Regalías), and Gobernación del Valle del Cauca. The authors acknowledge the China-Brazil Joint Laboratory for Space Weather (CBJLSW) for Supporting this Book Chapter. Vania F. Andrioli would like to thank the CBJLSW and the National Space Science Center (NSSC) of the Chinese Academy of Sciences (CAS) for supporting her postdoctoral fellowship. The authors from the Universidad de Magallanes would like to acknowledge the financial support of the Japan Science and Technology Agency (JST) /Japan International Cooperation Agency (JICA), the Science and Technology Research Association for Sustainable Development (SATREPS) through the SAVERNet project; and the Program FONDECYT of the Chilean National Agency for Research and Development (ANID) through Project FONDECYT 11181335.

Conflict of interest

The authors declare no conflict of interest.

Author details

Eduardo Landulfo[1*], Alexandre Cacheffo[1,2], Alexandre Calzavara Yoshida[1,2], Antonio Arleques Gomes[1], Fábio Juliano da Silva Lopes[1,3], Gregori de Arruda Moreira[1,4,5], Jonatan João da Silva[1,6], Vania Andrioli[7,8], Alexandre Pimenta[7], Chi Wang[9], Jiyao Xu[9], Maria Paulete Pereira Martins[7], Paulo Batista[7], Henrique de Melo Jorge Barbosa[10,11], Diego Alves Gouveia[10,12], Boris Barja González[13], Felix Zamorano[13], Eduardo Quel[14], Clodomyra Pereira[15,16], Elian Wolfram[17,18], Facundo Ismael Casasola[15,16,19], Facundo Orte[18], Jacobo Omar Salvador[18], Juan Vicente Pallotta[18], Lidia Ana Otero[14,19], Maria Prieto[15,16], Pablo Roberto Ristori[14], Silvina Brusca[14], John Henry Reina Estupiñan[20,21], Estiven Sanchez Barrera[20], Juan Carlos Antuña-Marrero[22], Ricardo Forno[23], Marcos Andrade[23], Judith Johanna Hoelzemann[24], Anderson Guimarães Guedes[25], Cristina Tobler Sousa[24], Daniel Camilo Fortunato dos Santos Oliveira[26,27], Ediclê de Souza Fernandes Duarte[27], Marcos Paulo Araújo da Silva[26,27] and Renata Sammara da Silva Santos[1,24]

1 Center for Lasers and Applications (CELAP), Institute of Energy and Nuclear Research (IPEN) Sao Paolo, Brazil

2 Institute of Exact and Natural Sciences of Pontal (ICENP), Federal University of Uberlândia (UFU), Ituiutaba, Brazil

3 Institute of Environmental, Chemical and Pharmaceutical Sciences (ICAQF), Federal University of São Paulo (UNIFESP), Diadema, Brazil

4 Federal Institute of São Paulo (IFSP), Campus Registro, Sao Paolo, Brazil

5 Institute of Astronomy, Geophysics and Atmospheric Sciences (IAG), University of São Paulo (USP), Sao Paolo, Brazil

6 Center for Exact Sciences and Technologies (CCET), Federal University of Western Bahia (UFOB), Barreiras, Brazil

7 National Institute for Space Research (INPE), São José dos Campos, Brazil

8 China-Brazil Joint Laboratory for Space Weather (NSSC/INPE), São José dos Campos, Brazil

9 State Key Laboratory of Space Weather (SKSW), National Space Science Center (NSSC), Chinese Academy of Sciences (CAS), Beijing, China

10 Physics Institute, University of São Paulo (USP), Sao Paolo, Brazil

11 Physics Department, University of Maryland Baltimore County (UMBC), Baltimore, USA

12 Royal Netherlands Meteorological Institute (KNMI), De Bilt, The Netherlands

13 Department of Mathematics and Physics, University of Magallanes (UMAG), Punta Arenas, Chile

14 Institute of Scientific and Technical Research for Defense (CITEDEF) - UNIDEF (MINDEF – CONICET), Buenos Aires, Argentina

15 Military Geographical Service, National Geographic Institute (IGN), Buenos Aires, Argentina

16 General Directorate of Research and Development of the Argentine Army (DIGID), Buenos Aires, Argentina

17 Argentine National Weather Service (SMN), Buenos Aires, Argentina

18 Laser and Applications Research Center (CEILAP), UNIDEF (MINDEF–CONICET), Buenos Aires, Argentina

19 Argentine National Defense University (UNDEF), Army Engineering Faculty (FIE), Buenos Aires, Argentina

20 Centre for Bioinformatics and Photonics (CIBioFi), Universidad del Valle (UniValle), Cali, Colombia

21 Physics Department, Universidad del Valle (UniValle), Cali, Colombia

22 Department of Theoretical, Atomic and Optical Physics, University of Valladolid (UVA), Valladolid, Spain

23 Department of Physics, Major University of San Andrés (UMSA), La Paz, Bolivia

24 Department of Atmospheric and Climate Sciences (DCAC), Federal University of Rio Grande do Norte (UFRN), Natal, Brazil

25 School of Science and Technology (ECT), Federal University of Rio Grande do Norte (UFRN), Natal, Brazil

26 Polytechnic University of Catalonia (UPC), Barcelona, Spain

27 Graduate Program in Climate Sciences, Federal University of Rio Grande do Norte (UFRN), Natal, Brazil

*Address all correspondence to: landulfo@gmail.com; elandulf@ipen.br

IntechOpen

© 2020 The Author(s). Licensee IntechOpen. This chapter is distributed under the terms of the Creative Commons Attribution License (http://creativecommons.org/licenses/by/3.0), which permits unrestricted use, distribution, and reproduction in any medium, provided the original work is properly cited. CC BY

References

[1] Barbosa, H. M. J., Barja, B., Pauliquevis, T., Gouveia, D. A., Artaxo, P., Cirino, G. G., Santos, R. M. N., Oliveira A. B., 2014: A permanent Raman lidar station in the Amazon: Description, characterization and first results. Atmos. Meas. Tech., v. 7, Issue 6, 1745-1762. https://doi.org/10.5194/amt-7-1745-2014.

[2] Landulfo, E., Papayannis, A., Artaxo, P., Castanho, A. D. A., de Freitas, A. Z., Souza, R. F., Vieira Junior, N. D., Jorge, M. P., Sánchez-Ccoyllo, O. R., Moreira, D. S., 2003: Synergetic measurements of aerosols over São Paulo, Brazil using LIDAR, sunphotometer and satellite data during the dry season, Atmos. Chem. Phys., v. 3, Issue 5, 1523-1539. https://doi.org/10.5194/acp-3-1523-2003.

[3] Landulfo, E., Matos, C. A., Torres, A. S., Sawamura, P., Uehara, S. T., 2007: Air quality assessment using a multi-instrument approach and air quality indexing in an urban area. Atmos. Res., v. 85, Issue 1, 98-111. https://doi.org/10.1016/j.atmosres.2006.11.008.

[4] Landulfo, E., Jorge, M. P. M. P., Held, G., Guardani, R., Steffens, J., Pinto, S. A. F., et al., 2010: Lidar observation campaign of sugar cane fires and industrial emissions in the State of São Paulo, Brazil. Proceedings of SPIE - The International Society for Optical Engineering. 7832. Lidar Technologies, Techniques, and Measurements for Atmospheric Remote Sensing VI. https://doi.org/10.1117/12.866078.

[5] Landulfo, E., Costa, R. F., Rodrigues, P., Lopes, F. J. S., 2004: Raman lidar characterization using a reference lamp. Proc. SPIE, Lidar Technologies, Techniques, and Measurements for Atmospheric Remote Sensing X, v. 9246. https://doi.org/10.1117/12.2057376.

[6] Oliveira, A. M., Sousa, C. T., Oliveira, N. P. M., Melo, A. K. S., Lopes, F. J. S., Landulfo, E., Elbern, H., Hoelzemann, J. J., 2019: Analysis of Atmospheric Aerosol Optical Properties in the Northeast Brazilian Atmosphere with Remote Sensing Data from MODIS and CALIOP/CALIPSO Satellites, AERONET Photometers and a Ground-Based Lidar. Atmosphere, v. 10, Issue 10, 594-615. https://doi.org/10.3390/atmos10100594.

[7] Guedes, A. G., Landulfo, E., Montilla-Rosero, E., Lopes, F. J. S., Hoelzemann, J. J., Fernandez, J. H., et al., 2018: Detection of Saharan mineral dust aerosol transport over Brazilian northeast through a depolarization lidar. EPJ Web of Conferences, v. 176, 05036. https://doi.org/10.1051/epjconf/201817605036.

[8] The European Aerosol Research Lidar Network: EARLINET. Available from http://www.earlinet.org. Accessed 30 October 2020.

[9] The National Institute for Research and Development for Optoelectronics (INOE), Romania. Remote Sensing. International Projects. About APEL. Available from: http://environment.inoe.ro/article/237/about-apel. Accessed 30 October 2020.

[10] Lopes, F. J. S., Moreira, G. A., Guerrero-Rascado, J. L., Silva, J. A., Gouveia, D. A., Gomes, A., Belegante, L., Freudenthaler, V., et al., 2018: Improving the Instrument and Analysis Capabilities of the São Paulo LALINET Lidar Station in the Framework of the APEL Project. In: 1st European Lidar Conference ELC2018, Thessaloniki, Greece. Available from: http://www.fap.if.usp.br/~hbarbosa/uploads/Site/Publications/Fabio_elc2018.pdf. Accessed 30 October 2020.

[11] Nicolae, D., Guerrero-Rascado, J. L., Belegante, L., Freudenthaler, V., Landulfo, E., Lopes, F. J. S.,

Alados-Arboledas, L., et al., 2018: APEL: Assessment of atmospheric optical Properties during biomass burning Events and Long-range transport of desert dust. Alcantara Study Executive Summary. ESA Contract N. 4000117289. Available from: https://nebula.esa.int/sites/default/files/neb_study/1317/C4000117289ExS.pdf. Accessed 30 October 2020.

[12] D'Amico, G., Amodeo, A., Baars, H., Binietoglou, I., Freudenthaler, V., Mattis, I., Wandinger, U., Pappalardo, G., 2015: EARLINET Single Calculus Chain – overview on methodology and strategy. Atmos. Meas. Tech., v. 8, Issue 11, 4891-4916. https://doi.org/10.5194/amt-8-4891-2015.

[13] D'Amico, G., Amodeo, A., Mattis, I., Freudenthaler, V., Pappalardo, G., 2016: EARLINET Single Calculus Chain – technical – Part 1: Pre-processing of raw lidar data. Atmos. Meas. Tech., v. 9, Issue 2, 491-507. https://doi.org/10.5194/amt-9-491-2016.

[14] Mattis, I., D'Amico, G., Baars, H., Amodeo, A., Madonna, F., Iarlori M., 2016: EARLINET Single Calculus Chain – technical – Part 2: Calculation of optical products. Atmos. Meas. Tech., v. 9, Issue 7, 3009-3029. https://doi.org/10.5194/amt-9-3009-2016.

[15] Wiedensohler, A., Andrade, M., Weinhold, K., Müller, T., Birmili, W., Velarde, et al., 2018: Black carbon emission and transport mechanisms to the free troposphere at the La Paz/El Alto (Bolivia) metropolitan area based on the Day of Census (2012), Atmos. Environ., v. 194, 158-169. https://doi.org/10.1016/j.atmosenv.2018.09.032.

[16] Stull, R. B., 1988: An Introduction to Boundary Layer Meteorology. Atmospheric and Oceanographic Sciences Library, v. 13. Springer, Dordrecht. ISBN: 978-90-277-2769-5. https://doi.org/10.1007/978-94-009-3027-8.

[17] Holzworth, C. G., 1964: Estimates of mean maximum mixing depths in the contiguous United States. Month. Weath. Rev., v. 92, Issue 5, 235-242. https://doi.org/10.1175/1520-0493(1964)092<0235:EOMMMD>2.3.CO;2.

[18] Zeng X., Brunke, M. A., Zhou, M., Fairall, C., Bond, N. A., Lenschow, D. H., 2004: Marine atmospheric boundary layer height over the eastern Pacific: data analysis and model evaluation. J. Climate, v. 17, Issue 21, 4159-4170. https://doi.org/10.1175/JCLI3190.1.

[19] Seidel, D. J., Ao, C. O., Li, K., 2010: Estimating climatological planetary boundary layer heights from radiosonde observations: Comparison of methods and uncertainty analysis. J. Geophys. Res., v. 115, Issue D16, D16113. https://doi.org/10.1029/2009JD013680.

[20] Emeis, S., Schäfer, K., Münkel, C., 2008: Surface-based remote sensing of the mixing-layer height - a review. Meteorologische Zeitschrift, v. 17, Issue 5, 621-630. https://doi.org/10.1127/0941-2948/2008/0312.

[21] Moreira, G. A., Landulfo, E., Peres, L. V., Mariano, G., Borayou, R., 2013: Obtenção da altura da Camada Limite Planetária a partir do Método das Imagens (In Portuguese). Rev. Ciência e Natura. Santa Maria, Brazil. Special Edition, 335 - 338. ISSN-e: 2179-460X. https://doi.org/10.5902/2179460X11645.

[22] Moreira, G. A., Lopes, F. J. S., Held, G., Albuquerque, T. T. A., Reis Junior, N. C., Borayou, R., Landulfo, E., 2013: Automatic methods to detect the top of the Atmospheric Boundary Layer. Proc. Lidar Technologies, Techniques, and Measurements for Atmospheric Remote Sensing IX. 88940T. https://doi.org/10.1117/12.2028750.

[23] Nisperuza, D. J., 2014: Lidar measurements and wavelet covariance transform method to estimate the

atmospheric boundary layer heights in Medellín, Colombia. Ópt. Pura y Aplicada, v. 47, Issue 2, 123-130. https://doi.org/10.7149/opa.47.2.123.

[24] Moreira, G. A., Marques, M. T. A., Nakaema, W., Moreira, A. C. de C. A., Landulfo, E., 2015: Planetary Boundary Layer height estimation from Doppler wind lidar measurements, radiosonde and HYSPLIT model comparison. Óptica Pura e Aplicada, v. 48, Issue 3, 179-183. ISSN-e 2171-8814. https://doi.org/10.7149/OPA.48.3.179.

[25] Moreira, G. A., Marques, M. T. A., Nakaema, W., Moreira, A. C. de C. A., Landulfo, E., 2015: Detecting the planetary boundary layer height from low-level jet with Doppler lidar measurements. Proc. SPIE 9645: Lidar Technologies, Techniques, and Measurements for Atmospheric Remote Sensing XI. 96450F. https://doi.org/10.1117/12.2195278.

[26] Salvador, N., Loriato, A. G., Santiago, A., Albuquerque, T. T. A., Reis Jr., N. C., Santos, J. M., et al., 2016: Study of the Thermal Internal Boundary Layer in Sea Breeze Conditions Using Different Parameterizations: Application of the WRF Model in the Greater Vitória Region. Rev. Bras. Meteorol., v. 31, Issue 4, 593 - 609. http://doi.org/10.1590/0102-7786312314b20150093.

[27] Céspedes, J., Melo-Luna, C. A., Reina, J. H., 2018: A first measurement of the planetary boundary layer top in Santiago de Cali - Colombia: elastic LiDAR application. Proc. Remote Sensing of Clouds and the Atmosphere XXIII. 107860L. https://doi.org/10.1117/12.2503534.

[28] Marques, M. T . A., Moreira, G. A., Piñero, M., Oliveira, A. P., Landulfo, E., 2018: Estimating the planetary boundary layer height from radiosonde and doppler lidar measurements in the city of São Paulo – Brazil, EPJ Web Conf., v. 176, 06015. https://doi.org/10.1051/epjconf/201817606015.

[29] Herrera-Mejía, L., Hoyos, C. D., 2019: Characterization of the atmospheric boundary layer in a narrow tropical valley using remote-sensing and radiosonde observations and the WRF model: the Aburrá Valley case-study. Q. J. R. Meteorol. Soc., v. 145, Issue 723, 2641 – 2665. https://doi.org/10.1002/qj.3583.

[30] Moreira, G. A., Lopes, F. J. S., Guerrero-Rascado, J. L., da Silva, J. J., Gomes, A., A., Landulfo, E., Alados-Arboledas, L., 2019: Analyzing the atmospheric boundary layer using high-order moments obtained from multiwavelength lidar data: impact of wavelength choice. Atmos. Meas. Tech., v. 12, Issue 8, 4261-4276. https://doi.org/10.5194/amt-12-4261-2019.

[31] Vivas, D. R., Sánchez, E., Reina, J. H., 2020: Deep learning the atmospheric boundary layer height. arXiv. preprint. arXiv: 2004.04353v1 [physics.ao-ph]. Available from: https://arxiv.org/pdf/2004.04353.pdf. Accessed 15 October 2020.

[32] Hayden, K., Anlauf, K., Hoff, R., Strapp, J., Bottenheim, J., Wiebe, H., et al., 1997: The vertical chemical and meteorological structure of the boundary layer in the Lower Fraser Valley during Pacific'93. Atmospheric Environment, v. 31, Issue 14, 2089-2105. https://doi.org/10.1016/S1352-2310(96)00300-7.

[33] Menut, L., Flamant, C., Pelon, J., Flamant, P. H., 1999: Urban boundary-layer height determination from lidar measurements over the Paris area. Applied Optics, v. 38, Issue 6, 945-954. https://doi.org/10.1364/AO.38.000945.

[34] Brooks, I. M., 2003: Finding boundary layer top: Application of a wavelet covariance transform to lidar backscatter profiles. Journal

of Atmospheric and Oceanic Technology, v. 20, Issue 8, 1092-1105. https://doi.org/10.1175/1520-0426(2003)020<1092:FBLTAO>2.0.CO;2.

[35] D'Almeida, G. A., Koepke, P., Shettle. E. P., 1991: Atmospheric aerosols: Global climatology and radiative characteristics. A. Deepak Publishing, Hampton, Virginia. ISBN-10: 0937194220.

[36] Australian Government. Bureau of Meteorology, 2019: Special Climate Statement 70 update – drought conditions in Australia and impact on water resources in the Murray–Darling Basin. Published 29 November 2019. Available from: http://www.bom.gov.au/climate/current/statements/scs70b.pdf. Accessed 20 October 2020.

[37] Randerson, J. T., Chen, Y., van der Werf, G. R., Rogers, B. M., Morton, D. C., 2012: Global burned area and biomass burning emissions from small fires. J. Geophys. Res., v. 117, G04012. https://doi.org/10.1029/2012JG002128.

[38] Suomi NPP (National Polar-orbiting Partnership) Mission. Available from: https://earth.esa.int/web/eoportal/satellite-missions/s/suomi-npp. The ESA Earth Observation Portal (eoPortal). Accessed 20 October 2020.

[39] OMPS-NPP L2 NM Aerosol Index swath orbital V2. Available from: https://disc.gsfc.nasa.gov/datasets/OMPS_NPP_NMMIEAI_L2_2/summary. Accessed 20 October 2020.

[40] Moderate Resolution Imaging Spectroradiometer (MODIS). Available from: https://modis.gsfc.nasa.gov. Accessed 20 October 2020.

[41] Levy, R. C., Mattoo, S., Munchak, L. A., Remer, L. A., Sayer, A. M., Patadia, F., Hsu, N. C., 2013: The Collection 6 MODIS aerosol products over land and ocean. Atmospheric Measurement Techniques, v. 6, 2989-3034. https://doi.org/10.5194/amt-6-2989-2013.

[42] Apituley, A., Pedergnana, M., Sneep, M., Pepijn Veefkind, J., Loyola, D., Landgraf, J., Borsdorff, T., 2018: Sentinel-5 precursor/TROPOMI Level 2 Product User Manual Carbon Monoxide. Royal Netherlands Meteorological Institute (KNMI). Document Number: SRON-S5P-LEV2-MA-002. Available from: https://sentinel.esa.int/documents/247904/2474726/Sentinel-5P-Level-2-Product-User-Manual-Carbon-Monoxide. Accessed 20 October 2020.

[43] Torres, O., Bhartia, P. K., Herman, J. R., Ahmad, Z., Gleason, J., 1998: Derivation of aerosol properties from satellite measurements of backscattered ultraviolet radiation: Theoretical basis. Journal Geophys. Res., v. 103, Issue D14, 17099 – 17110. https://doi.org/10.1029/98JD00900.

[44] Holben, B. N., Eck, T. F., Slutsker, I., Tanré, D., Buis, J. P., Setzer, A., et al., 1998: AERONET - A federated instrument network and data achieve for aerosol characterization. Remote Sens. of Environ., v. 66, Issue 1, 1-16. https://doi.org/10.1016/S0034-4257(98)00031-5.

[45] Dubovik, O., King, M., 2000: A flexible inversion algorithm for retrieval of aerosol optical properties from Sun and sky radiance measurements. J. Geophys. Res., v. 105, Issue D16, 20673-20696. https://doi.org/10.1029/2000JD900282.

[46] Otero L., Ristori, P., Holben, B., Quel, E., 2006: Aerosol Optical Thickness at ten AERONET – NASA stations during 2002 (In Spanish). Opt. Pura y Apl. v. 39, Issue 4, 355-364. Sociedad Española de Óptica. Available from: https://www.sedoptica.

es/Menu_Volumenes/Pdfs/228.pdf. Accessed 20 October 2020.

[47] Ristori, P., Otero, L., Jin, Y., Barja, B., Shimizu, A., Barbero, A., Salvador, J., Bali, J. L., Herrera, M., Etala, P., Acquesta, A., Quel, E., Sugimoto, N., Mizuno, A., 2018: Saver.net lidar network in southern South America. The 28th International Laser Radar Conference (ILRC 28). EPJ Web Conf., v. 176, 09011. https://doi.org/10.1051/epjconf/201817609011.

[48] Otero L., Ristori, P., Holben, B. N., Quel, E., 2006: Aerosol optical properties by means of a sunphotometer and lidar system in Buenos Aires, Argentina. Opt. Pura y Apl., Especial III Workshop on Lidar Measurements in Latin America, v. 39, n. 1, 43 – 47. Sociedad Española de Óptica. e-ISSN: 2171-8814. Available from: https://www.sedoptica.es/Menu_Volumenes/Pdfs/183.pdf. Accessed 20 October 2020.

[49] Otero, L., Ristori, P., Pawelko, E., Pallotta, J., Quel, E., 2011: Six-Year Evolution of Multiwavelength Lidar System at CEILAP. Opt. Pura y Apl., V Workshop on Lidar Measurements in Latin America, v. 44, 13 – 18. Sociedad Española de Óptica. ISSN 0030-3917. Available from: https://www.sedoptica.es/Menu_Volumenes/Pdfs/OPA44-1-13.pdf. Accessed 20 October 2020.

[50] Landgraf, J., aan de Brugh, J., Scheepmaker, R., Borsdorff, T., Hu, H., Houweling, S., Butz, A., Aben, I., and Hasekamp, O., 2016: Carbon monoxide total column retrievals from TROPOMI shortwave infrared measurements. Atmos. Meas. Tech., v. 9, 4955-4975. https://doi.org/10.5194/amt-9-4955-2016.

[51] Otero L., Casasola, F., Pereyra, C., Prieto, M., Brusca, S., Ristori, P., 2020: Australian Aerosol Layers Over Argentine Territory During November 2019 (In Spanish). Asociación Física Argentina. Anales AFA, v. 31, n. 1, 1-6. ISSN : 1850-1168. https://doi.org/10.31527/analesafa.2020.31.1.1.

[52] Mahowald, N. M., Ballantine, J. A., Feddema, J., and Ramankutty, N., 2007: Global trends in visibility: implications for dust sources. Atmos. Chem. Phys., v. 7, Issue 12, 3309-3339. https://doi.org/10.5194/acp-7-3309-2007.

[53] Prospero, J. M., Collard, F-X., Molinié, J., Jeannot, A., 2014: Characterizing the annual cycle of African dust transport to the Caribbean Basin and South America and its impact on the environment and air quality. Global Biogeochemical Cycles, v. 28, Issue 7, 757-773. https://doi.org/10.1002/2013GB004802.

[54] Zender, C. S., Miller, R. L. R. L., Tegen, I., 2004: Quantifying mineral dust mass budgets: Terminology, constraints, and current estimates. EOS. Science News by AGU, v, 85, Issue 48, 509-512. https://doi.org/10.1029/2004EO480002.

[55] Mona L, Liu Z, Müller D, Omar A, Papayannis A, Pappalardo G, et al. Lidar Measurements for Desert Dust Characterization: An Overview. Advances in Meteorology, v. 2012, Article ID 356265. In: Special Issue. Desert Dust Properties: Modelling, and Monitoring; 2012 https://doi.org/10.1155/2012/356265

[56] Bristow, C. S., Hudson-Edwards, K. A., Chappell, A., 2010: Fertilizing the Amazon and equatorial Atlantic with West African dust. Geophysical Research Letters: Atmospheric Science, v. 37, Issue 14. https://doi.org/10.1029/2010GL043486.

[57] Ben-Ami, Y., Koren, I., Rudich, Y., Artaxo, P., Martin, S. T., and Andreae, M. O., 2010: Transport of North African dust from the Bodélé depression to the Amazon Basin: a case

study, Atmos. Chem. Phys., v. 10, Issue 16, 7533-7544. https://doi.org/10.5194/acp-10-7533-2010.

[58] Schulz, M., Prospero, J. M., Baker, A. R., Dentener, F., Ickes, L., Liss, P. S., et al., 2012: The atmospheric transport and deposition of mineral dust to the ocean: Implications for research needs. Environ. Sci. Technol., v. 46, Issue 19, 10390-10404. https://doi.org/10.1021/es300073u.

[59] Ben-Ami, Y., Koren, I., Altaratz, O., 2009: Patterns of Saharan dust transport over the Atlantic: Winter vs. Summer, based on CALIPSO first year data. Atmospheric Chemistry and Physics, v. 9, Issue 3, 7867-7865. https://doi.org/10.5194/acpd-9-13177-2009.

[60] Oliveira, D. C. F. S., Montilla-Rosero, E., Lopes, F. J. S., Morais, F. G., Landulfo, E., Hoelzemann, J. H., 2020: Aerosol properties in the atmosphere of Natal/Brazil measured by an AERONET Sun-photometer. Environmental Science and Pollution Research. https://doi.org/10.1007/s11356-020-11373-z.

[61] Talbot, R. W., Andreae, M. O., Berresheim, H., Artaxo, P., Garstang, M., Harriss, R. C., Beechef, K. M., Li, S. M., 1990: Aerosol chemistry during the wet season in central Amazonia: The influence of long-range transport. J. Geophys. Res., v. 95, Issue D10, 16955-16969. https://doi.org/10.1029/JD095iD10p16955.

[62] Swap, R., Garstang, M., Greco, S., Talbot, R., Kållberg, P., 1992: Saharan dust in the Amazon Basin. Tellus B, v. 44, Issue 2, 133-149. https://doi.org/10.1034/j.1600-0889.1992.t01-1-00005.x.

[63] Landulfo, E., Lopes, F. J. S., Montilla, E., Guedes, A. G., Hoelzemann, J. J., Fernandez, J. H., Alados-Arboledas, L., Guerrero-Rascado, J. L., 2016: DUSTER lidar: transatlantic transport of aerosol particles from the Sahara and other sources: first results from the recently installed lidar and sunphotometer in Natal/Brazil. Proc. SPIE 10006, Lidar Technologies, Techniques, and Measurements for Atmospheric Remote Sensing XII, 1000607. https://doi.org/10.1117/12.2241386.

[64] Baars, H., Ansmann, A., Althausen, D., Engelmann, R., Artaxo, P., Pauliquevis, T., Souza, R., 2011: Further evidence for significant smoke transport from Africa to Amazonia. Geophysical Research Letters: Atmospheric Science, v. 38, Issue 20. https://doi.org/10.1029/2011GL049200.

[65] Abouchami, W., Näthe, K., Kumar, A., Galer, J. G., Jochum, K. P., Williams, E., et al., 2013: Geochemical and isotopic characterization of the Bodélé Depression dust source and implications for transatlantic dust transport to the Amazon Basin. Earth and Planetary Science Letters, v. 380, 112-123. https://doi.org/10.1016/j.epsl.2013.08.028.

[66] Rizzo, L. V., Artaxo, P., Müller, T., Wiedensohler, A., Paixão, M., Cirino, G. G., et al., 2013: Long term measurements of aerosol optical properties at a primary forest site in Amazonia. Atmos. Chem. Phys., v 13, Issue 5, 2391-2413, https://doi.org/10.5194/acp-13-2391-2013.

[67] Freudenthaler, V., 2016: About the effects of polarizing optics on lidar signals and the Delta 90 calibration. Atmospheric Measurement Techniques, v. 9, Issue 9, 4181-4255. ISSN: 1867-1381. https://doi.org/10.5194/amt-9-4181-2016.

[68] Van Hai, B., Van Trung, D., Xuan Tuan, N., Duy Thang, D., Thanh Binh, N., 2012: Monitoring cirrus cloud and tropopause height over Hanoi using a compact lidar system. Communications in Physics, v. 22, Issue 4. 357-364. ISSN: 0868-3166. https://doi.org/10.15625/0868-3166/22/4/2488.

[69] Heymsfield, A. J., Krämer, M., Luebke, A., Brown, P., Cziczo, D. J., Franklin, C., et al., 2017: Cirrus clouds. Meteorological Monographs, v. 58, 2.1-2.26. https://doi.org/10.1175/AMSMONOGRAPHS-D-16-0010.1.

[70] Guedes, A. G., 2019: Characterization of the transport of Saharan dust aerosols on Natal-RN using the lidar depolarization technique [thesis] (In Portuguese). Center for Exact and Earth Sciences. Graduate Program in Climate Sciences. Federal University of Rio Grande do Norte. Available from: https://repositorio.ufrn.br/handle/123456789/27386. Accessed 6 November 2020.

[71] Boucher, O., Randall, D., Artaxo, P., Bretherton, C., Feingold, G., Forster, P., et al., 2013: Clouds and Aerosols. In Climate Change 2013: The Physical Science Basis. Contribution of Working Group I to the Fifth Assessment Report of the Intergovernmental Panel on Climate Change. Editors: Stocker, T. F., Qin, D., Plattner, G.-K., Tignor, M., Allen, S. K., Boschung, J., Nauels, A., Xia, Y., Bex, V., and Midgley, P. M., Cambridge University Press, 571-658, https://doi.org/10.1017/CBO9781107415324.016.

[72] Sassen K, Wang Z, Liu D. Cirrus clouds and deep convection in the tropics: Insights from CALIPSO and CloudSat, J. Geophys. Res., v. 114, Issue D4. In: D00H06. 2009 https://doi.org/10.1029/2009JD011916

[73] Liou, K. N., 1986: Influence of cirrus clouds on weather and climate processes: A global perspective, Mon. Weather Rev., v. 114, Issue 6, 1167 – 1199. https://doi.org/10.1175/1520-0493(1986)114<1167:IOCCOW>2.0.CO;2.

[74] Kienast-Sjögren, E., Rolf, C., Seifert, P., Krieger, U. K., Luo, B. P., Krämer, M., and Peter, T., 2016: Climatological and radiative properties of midlatitude cirrus clouds derived by automatic evaluation of lidar measurements. Atmos. Chem. Phys., v. 16, Issue 12, 7605-7621. https://doi.org/10.5194/acp-16-7605-2016.

[75] Nazaryan, H., McCormick, M. P., and Menzel, W. P., 2008: Global characterization of cirrus clouds using CALIPSO data, J. Geophys. Res., v. 113, Issue D16, D16211. https://doi.org/10.1029/2007JD009481.

[76] Pandit, A. K., Gadhavi, H. S., Venkat Ratnam, M., Raghunath, K., Rao, S. V. B., and Jayaraman, A., 2015: Long-term trend analysis and climatology of tropical cirrus clouds using 16 years of lidar data set over Southern India, Atmos. Chem. Phys., v. 15, Issue 24, 13833-13848. https://doi.org/10.5194/acp-15-13833-2015.

[77] Lakkis, G. S., Lavorato, M., and Canziani, O. P., 2009: Monitoring cirrus clouds with lidar in the Southern Hemisphere: a local study over Buenos Aires. 1. Tropopause heights, Atmos. Res., v. 92, Issue 1, 18-26. https://doi.org/10.1016/j.atmosres.2008.08.003.

[78] Antuña, J. C., Barja, B., 2006: Cirrus clouds optical properties measured with lidar at Camagüey, Cuba. Óptica Pura y Aplicada, v. 39, Issue 1, 11-16. Proceedings of the Third Workshop of Lidar Measurements in Latin America. ISSN-e 2171-8814. Available from: https://www.sedoptica.es/Menu_Volumenes/Pdfs/178.pdf. Accessed 13 October 2020.

[79] Gouveia, D. A., Barja, B., Barbosa, H. M., Seifert, P., Baars, H., Pauliquevis, T., Artaxo, P., 2017: Optical and geometrical properties of cirrus clouds in Amazonia derived from 1 year of ground-based lidar measurements. Atmospheric Chemistry and Physics, v. 17, Issue 5, 3619-3636. https://doi.org/10.5194/acp-17-3619-2017.

[80] Santos, R. S. S., 2018: Study of physical properties of cirrus clouds in

Natal using data from the lidar-Duster system and radiosondes [capstone project] (In Portuguese). Technology Center. Federal University of Rio Grande do Norte. Brazil. Available from: http://monografias.ufrn.br/handle/123456789/6908. Accessed 13 October 2020.

[81] Larroza, E. G., 2011: Characterization of cirrus clouds over São Paulo Metropolitan City (MSP) by elastic lidar [thesis] (In Portuguese). Institute of Energy and Nuclear Research. University of São Paulo. Brazil. https://doi.org/10.11606/T.85.2011.tde-19122011-153154.

[82] Barja, B. et al. 2019: Cirrus cloud observations at the southern-hemispheric midlatitude site of Punta Arenas (53°S, 71°W). International Symposium on Tropospheric Profiling (ISTP), 20 - 24 May 2019. Météo-France - Toulouse - France. http://www.meteo.fr/cic/meetings/2019/ISTP/programme_ISTP11.pdf.

[83] Barja, B., Antuña, J. C., 2011: The effect of optically thin cirrus clouds on solar radiation in Camagüey, Cuba. Atmos. Chem. Phys., v. 11, Issue 16, 8625-8634. https://doi.org/10.5194/acp-11-8625-2011.

[84] Gouveia, D. A., 2018: Radiative forcing, physical and optical properties of cirrus clouds over Amazon [thesis] (In Portuguese). Institute of Physics. University of São Paulo. Brazil. https://doi.org/10.11606/T.43.2019.tde-08022019-141530.

[85] Emde, C., Buras-Schnell, R., Kylling, A., Mayer, B., Gasteiger, J., Hamann, U., et al., 2016: The libRadtran software package for radiative transfer calculations (version 2.0.1). Geoscientific Model Development, v. 9, Issue 5, 1647-1672. https://doi.org/10.5194/gmd-9-1647-2016.

[86] Barbosa, H. M. J., Gouveia, D. A., Kalese, H., Seifert, P., Barja, B., Monteiro, M., Correia, A., Pauliquevis, T., Ansmann, A., 2018: Optical Properties and Radiative Forcing of Cirrus Clouds in the Central Amazon Forest. X Workshop on Lidar Measurements in Latin America. Medellín, Colombia. Available from: http://www.fap.if.usp.br/~hbarbosa/uploads/Site/Publications/Barbosa_wlmla2018.pdf. Accessed 3 November 2020.

[87] Larroza, E. G., Nakaema, W. M., Bourayou, R., Hoareau, C., Landulfo, E., and Keckhut, P., 2013: Towards an automatic lidar cirrus cloud retrieval for climate studies. Atmos. Meas. Tech., v. 6, Issue 11, 3197-3210. https://doi.org/10.5194/amt-6-3197-2013.

[88] Bühl, J., Seifert, P., Wandinger, U., Baars, H., Kanitz, T., Schmidt, J., et al., 2013: LACROS: the Leipzig Aerosol and Cloud Remote Observations System. Proc. SPIE v. 8890. Remote Sensing of Clouds and the Atmosphere XVIII; and Optics in Atmospheric Propagation and Adaptive Systems XVI. 889002. https://doi.org/10.1117/12.2030911.